TiO$_2$ Photocatalysis for the Transformation of Aromatic Water Pollutants into Fuels

Osama Al-Madanat [1,2,*], Yamen AlSalka [1,3], Wegdan Ramadan [4] and Detlef W. Bahnemann [1,3,5,*]

1   Institut für Technische Chemie, Leibniz Universität Hannover, Callin str. 3, 30167 Hannover, Germany; alsalka@iftc.uni-hannover.de
2   Chemistry Department, Mutah University, Mutah, Al-Karak 61710, Jordan
3   Laboratorium für Nano- und Quantenengineering, Leibniz Universität Hannover, Schneiderberg 39, 30167 Hannover, Germany
4   Faculty of Science, Physics Department, Alexandria University, Alexandria 21511, Egypt; wegdan.ramadan@alexu.edu.eg
5   Laboratory "Photoactive Nanocomposite Materials", Saint-Petersburg State University, Ulyanovskaya str. 1, 198504 Saint-Petersburg, Russia
*   Correspondence: al-madanat@iftc.uni-hannover.de (O.A.-M.); bahnemann@iftc.uni-hannover.de (D.W.B.); Tel.: +49-511-762-2773 (O.A.-M.)

Abstract: The growing world energy consumption, with reliance on conventional energy sources and the associated environmental pollution, are considered the most serious threats faced by mankind. Heterogeneous photocatalysis has become one of the most frequently investigated technologies, due to its dual functionality, i.e., environmental remediation and converting solar energy into chemical energy, especially molecular hydrogen. H$_2$ burns cleanly and has the highest gravimetric gross calorific value among all fuels. However, the use of a suitable electron donor, in what so-called "photocatalytic reforming", is required to achieve acceptable efficiency. This oxidation half-reaction can be exploited to oxidize the dissolved organic pollutants, thus, simultaneously improving the water quality. Such pollutants would replace other potentially costly electron donors, achieving the dual-functionality purpose. Since the aromatic compounds are widely spread in the environment, they are considered attractive targets to apply this technology. In this review, different aspects are highlighted, including the employing of different polymorphs of pristine titanium dioxide as photocatalysts in the photocatalytic processes, also improving the photocatalytic activity of TiO$_2$ by loading different types of metal co-catalysts, especially platinum nanoparticles, and comparing the effect of various loading methods of such metal co-catalysts. Finally, the photocatalytic reforming of aromatic compounds employing TiO$_2$-based semiconductors is presented.

Keywords: TiO$_2$; aromatic compound; PAHs; H$_2$ production; photocatalytic reforming; water remediation

1. Introduction

Water is essential for the existence of all living beings. However, its pollution with organic and inorganic compounds remains a threat and poses great risks to the environment and human health. The water quality is merely a concept reflecting the kind and quantity of contaminants contained in it. Mining and petrochemical industries are instrumental in the economic growth of many countries and their products are regarded as privileges to modern communities [1]. However, the wastes generated from the activities of these industries are toxic and carcinogenic [2]. Thus, these wastes have been classified as "hazardous" [3], and there is a constant increase in the pollution concerns associated with various petrochemical compounds and their by-products in the form of water, air, and soil pollution. Many of these by-products are still extensively employed, especially in the chemical, medical, and other industrial fields, as irreplaceable and inevitable raw materials [4–7]. Aromatic compounds, such as benzene, phenol, and chlorobenzene,

are some of the most encountered volatile organic compounds (VOCs). The primary sources of VOCs are originated from a large number of anthropogenic activities, such as refinery streams, especially from catalytic reforming and cracking, and petroleum refining, petrochemical processing, and solvent use [8,9]. Other VOCs, such as methane and chlorofluorocarbons, are classified as "greenhouse gases", which cause global warming.

The aromatic ring is the basic constituent of many organic pollutants, such as polyaromatic hydrocarbons (PAHs), dyes, pesticides, and pharmaceuticals. Aromatic compounds, such as benzene, phenols, and benzoic acid, are the most frequently used model substrates to investigate the photocatalytic mechanism and to test the activity of the photocatalysts [10–13]. Detailed studies have been made on the harm caused by the aromatic compounds, for example, the potential relationship between the benzene-related compounds and the risk of hematologic cancers, such as lymphoid malignancies [14]. Moreover, long-term exposure to a low concentration of such compounds could predispose to the development of type 2 diabetes (T2D) and affect human metabolism [15,16]. Aromatic organic compounds also contribute to serious environmental problems, such as water pollution, which may result in the demise of scarce species, and biological genetic variation, which in many cases is an irreversible problem [17,18].

Semiconductor photocatalysis has been extensively studied in the past 30 years as a promising method of environmental cleanup and sterilization. However, an earlier description of the photocatalytic properties of some metal oxides was given in 1955 by Markham [19], who dealt with ZnO, Sb_2O_3, and TiO_2, and the various types of photochemical changes that these oxides could undergo, including the catalyzed oxidation of organic compounds under UV irradiation. Later, and in 1972, a short note published in *Nature* by Fujishima and Honda [20] demonstrated that water could be photolyzed electrochemically at an illuminated TiO_2 and Pt electrode combination to yield stoichiometric quantities of H_2 and O_2. What followed soon thereafter was a frenzied series of studies in search of the photocatalytic materials to produce H_2 fuel as part of the beginnings of the hydrogen economy. Many semiconductors showed photocatalytic properties like MoS_2 [21], WO_3 [22], $BiFeO_3$ [23], Fe_2O_3 [24], and $CdTe$ [25,26], but only a few of them fulfill the thermodynamic requirements for overall water splitting, such as $KTaO_3$, $SrTiO_3$, TiO_2, ZnS, and SiC. What seems a simple basic function like the excitation of the semiconductor by absorption of light results in the formation of the charge carrier, i.e., the valence band holes, h_{vb}^+, and the conduction band electrons, e_{cb}^-. However, because of the strong oxidation ability of h_{vb}^+ and reactive oxygen species like $^\bullet OH$, $^\bullet OOH$, and H_2O_2, which are formed from the h_{vb}^+ oxidation of H_2O and e_{cb}^- reduction of O_2, most organic compounds can be oxidized, even mineralized to CO_2 and H_2O in the photocatalytic systems. Due to the challenges that remain in achieving overall pure water splitting, the alternative approach is to combine light-induced splitting of water and photooxidation of organic substrates into a single process in so-called photocatalytic reforming [27].

TiO_2 is one of the most studied photocatalysts, it was greatly debated in many aspects like the nature of the oxidative agent ($^\bullet OH$ radicals vs. h^+), the site at which the reaction takes place (surface versus bulk solution), how to improve performance, and efficiency of TiO_2 photocatalytic properties. Unfortunately, TiO_2 has a relatively large bandgap (3.2 eV) so that only UV radiation can activate it, its conduction band is somewhat positive in relation to the redox potential for H_2 evolution. Clearly, new semiconductor-based nanostructured materials are needed that would use lower-energy photons available in the visible spectral region. A strategy developed mostly in the past decade was to push the absorption onset of TiO_2 toward longer wavelengths ($\geq$387 nm) by doping TiO_2 with anions and/or cations (N, C, S, F,..., and metal ions) [28]. Despite the many studies carried out with TiO_2, no other metal oxide has yet been found that might act as an efficient photoanode with conduction and valence band edges that straddle the redox potentials of water and many water organic pollutants.

In the first part of this review, we discuss the different classes of aromatic organic hydrocarbons pollutants with an emphasis on their chemical, structural, and physical

properties. Their environmental hazards, health threats, and their ability to leak into the different components of the environment especially the aquatic environment are also discussed. In the following parts of this review, we provide the reader with an overview of the conventional methods adopted for the treatment of organic pollutants against the recent methods used and the new trends to be evaluated and debated. The fundamental and electronic structure of semiconductor–photocatalyst, the significant parameters affecting its performance, and photocatalytic water splitting versus photocatalytic reforming are reviewed in detail. The next part of this review is dedicated to TiO_2, which is one of the most widely studied semiconductors, with emphasis on the photocatalytic properties of its different phases and how to enhance the performance of pristine TiO_2 by the loading of noble metals. Finally, and based on the recent research investigations, the current perspective for photocatalytic reforming of aromatic-based pollutants towards H_2 production and water decontamination is reviewed and highlighted.

2. Aromatic Hydrocarbons as Water Pollutants

Many pollutants discarded into the environment contain non-degradable substances like heavy metals and organic pollutants [29–31]. The persistent organic pollutants, such as pesticides [32], aromatic organic compounds (OCs) [33,34], semi-volatile organic compounds (SVOCs) [35–37], and organic dyes [38,39] are gaining great environmental concerns due to their impacts on health and environment. These compounds have grasped much attention due to their carcinogenic potential and ubiquitous presence in the environment, which pose a major threat to water reservoirs and the surrounding ecosystem.

The aromatic organic compounds, such as benzene, toluene, ethylbenzene, and xylenes (BTEX), polyaromatic hydrocarbons (PAHs), phenols, and their derivatives are frequently detected in different wastewater resources [40]. The removal of these organic pollutants is a must to reuse this water since such pollutants cannot be eliminated efficiently during conventional treatment processes. The reuse of this treated water, especially in irrigation of crops, contains great risks due to the transfer of these pollutants to plants, thus, through the food chain to living organisms [32,35]. The following subsections provide a brief description of the main types of these pollutants.

2.1. Phenols

Phenolic compounds are a class of organic compounds that consists of a hydroxyl group(s) directly bonded to one or more aromatic rings. The phenolic compounds are classified as priority pollutants due to their carcinogenic, mutagenic properties, and high toxicity even at low concentrations [41]. These compounds represent serious threats to human health, e.g., skin and eye irritations, anemia, respiratory, and vertigo [42]. The Environmental Protection Agency (EPA) sets the level standard of phenols in the surface water to less than 1 $\mu g \cdot L^{-1}$, while, the toxicity levels for both humans and aquatic life are usually in the range 9–25 $mg \cdot L^{-1}$ [41]. Phenols are one of the main intermediates for household and industrial productions of cleaners, dyes, pesticides, herbicides, paint, pharmaceuticals, petrochemicals, cooking operations, resin manufacturing, plastics, pulp, paper, and wood products [33,42]. They are usually detected in the wastewater effluents in very high concentrations up to thousands of $mg \cdot L^{-1}$ [43].

The first member of this category of organic compounds is phenol with the chemical formula of C_6H_5OH. All other members of the group are derivatives of phenol [44]. Chlorophenols are the largest group and most spread group of phenols. They are formed in the environment by chlorination of mono and polyaromatic compounds present in soil and water [42]. Moreover, the reaction of hypochlorite with phenolic acids during the treatments and disinfection processes leads to the formation of such chlorinated compounds. Chlorinated phenols, e.g., 2-chlorophenol, 2,4-dichlorophenol, 2,4,6-trichlorophenol, and pentachlorophenol (Chart 1), are listed by the U.S. EPA as priority organic pollutants [45,46].
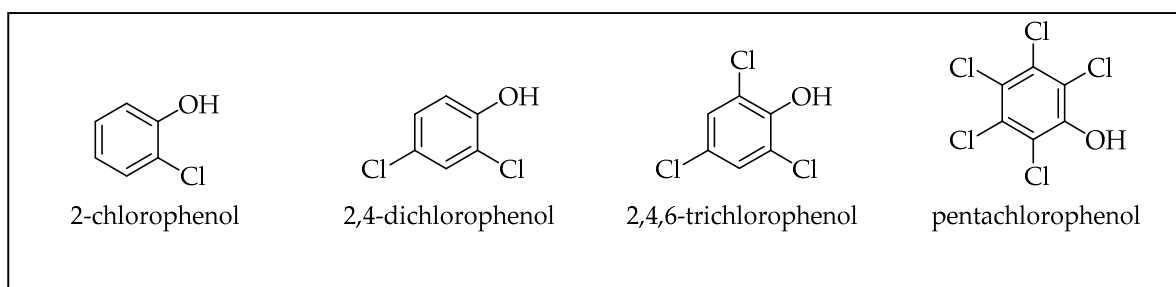
Chart 1. Common priority pollutant phenols.

2.2. Polyaromatic Hydrocarbons

Another kind of organic pollutants that causes water contamination is the PAHs, which are classified as hazardous persistent environmental pollutants [47]. They are a group of over 100 different organic compounds containing two or more fused aromatic benzene rings connected linearly, angularly, or in a cluster arrangement [48,49]. PAHs are found naturally and released into the environment by anthropogenic sources. The incomplete combustion of wood, coal, oil, gas, garbage, and other organic substances, pyrosynthesis or pyrolysis of hydrocarbons (petrogenesis), and the leakage of crude oil and refined petroleum products are considered the main sources of the PAHs [47,50,51]. The surface runoff from roads is another major source of the PAHs in the aquatic system [52,53]. Surface-active compounds and humic substances increase the solubility of PAHs several times. Huang and Buekens [54] reported the formation of the PAHs under insufficient combustion conditions of the aliphatic fuels. Under these conditions, carbon containing-compounds are not oxidized completely to carbon dioxide, rather, hydrocarbon fragments that are generated during incomplete combustion interact with each other to yield complex polycyclic structures. Many other resources for the PAHs [49,53] are shown in Figure 1.
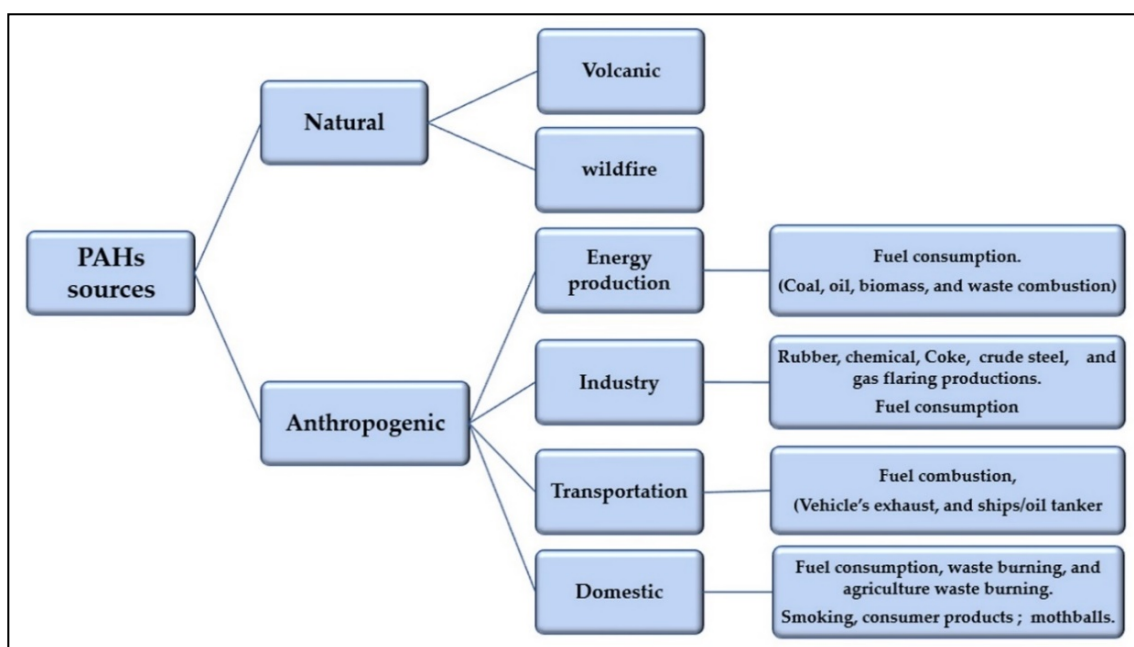

Figure 1. Different sources of polyaromatic hydrocarbons (PAHs) generation.

PAHs have low aqueous solubility and are considered as lipophilic organic compounds that are widely distributed in the environment and characterized by their high toxicity, genotoxicity, and carcinogenicity. [49,55]. Table 1 shows the physicochemical properties of 16 compounds of the PAHs that have been listed as priority pollutants by the United

States Environmental Protection Agency [50,56]. PAHs of two and three aromatic rings, e.g., naphthalene and anthracene, are known as low molecular weight (LMW). Those compounds possess higher solubility in water and higher volatility than that of the high molecular weight (HMW) PAHs [57]. In fact, higher concentrations of the LMW PAHs have been reported in wastewater influent and effluent comparing to the HMW PAHs, which can be related to their higher water solubility [35,40,58–61].

Naphthalene ($C_{10}H_8$) is the simplest form of PAHs and possesses higher volatility besides its higher solubility in water (31.7 mg·L^{-1} at 25 °C) compared to other PAH compounds. Naphthalene is widely used in industry as an intermediate in the production of pesticides, phthalic anhydride, dyes, resins, and surfactants [62,63]. Moreover, it is found in many consumer products like mothballs and some insect repellent products that are used to kill moths in airtight spaces, and to repel vertebrate pests in attics and wall voids spaces [64]. In general, naphthalene was found the most ubiquitous and abundant PAH in wastewater with concentrations ranged between ng·L^{-1} to μg·L^{-1} [47,59–61,65,66].

2.3. Organic Dyes

Dyes are colored substances that have an affinity for the substrate to which they are being applied. They have colors due to their absorption of light at a certain wavelength in the visible range. Due to their high molar extinction coefficients, a small amount of dye in an aqueous solution can produce a vivid color [67,68]. Synthetic dyes possess very different chemical and physical properties. Azo, anthraquinone, xanthene, indigoid, triphenylmethane, and phthalocyanine derivatives are the most frequent chemical classes of dyes employed in the industry (Chart 2) [67–71].
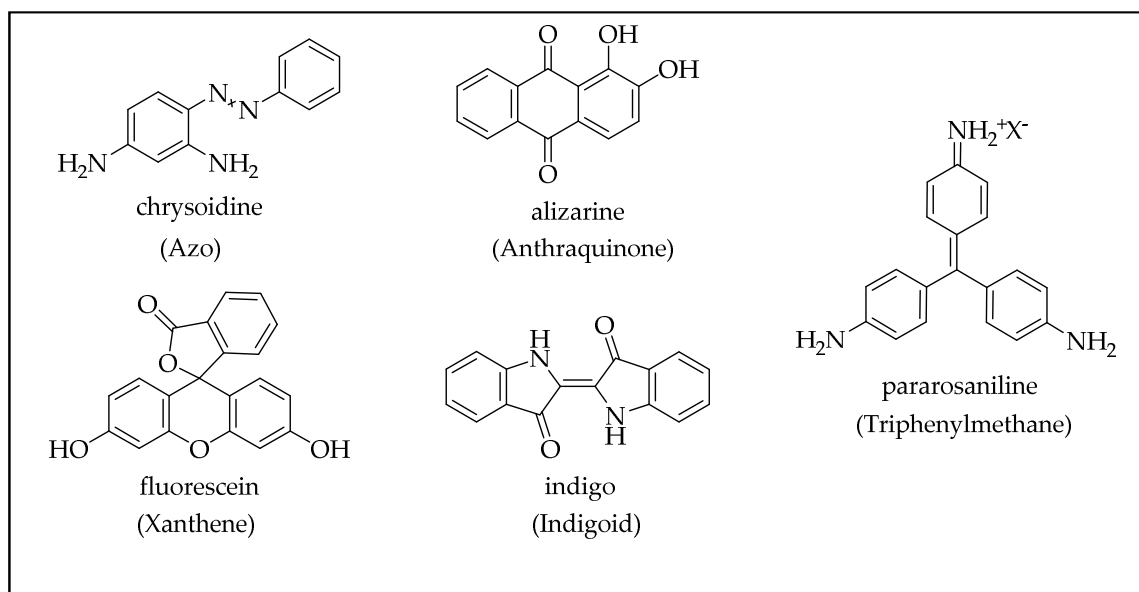

Chart 2. The chemical structures of some common synthetic dyes.

**Table 1.** Physiochemical properties of the 16 U.S. Environmental Protection Agency (EPA) PAHs [53,72,73].
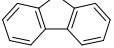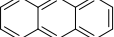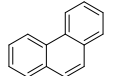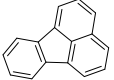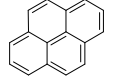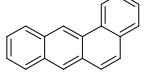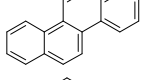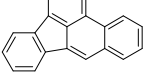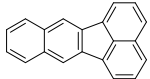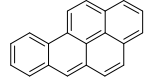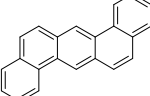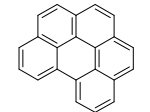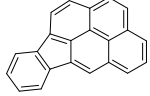
Compound Name	Chemical Structure	Chemical Formula	Number of Rings	Molecular Weight (g\mol)	Melting Point (°C)	Boiling Point (°C)	Aqueous Solubility (mg/L)	Vapor Pressure (Pa)	Log K_{ow}
Naphthalene		$C_{10}H_8$	2	128.17	80.26	218	31	1.0×10^2	3.37
Acenaphthene		$C_{12}H_{10}$	3	154.21	93.4	279	3.8	3.0×10^{-1}	3.92
Acenaphthylene		$C_{12}H_8$	3	152.19	92–93	265–275	16	9.0×10^{-1}	4.00
Fluorene		$C_{13}H_{10}$	3	166.22	116–117	295	1.9	9.0×10^{-2}	4.18
Anthracene		$C_{14}H_{10}$	3	178.23	218	340–342	0.045	1.0×10^{-3}	4.54
Phenanthrene		$C_{14}H_{10}$	3	178.23	100	340	1.1	2.0×10^{-2}	4.57
Fluoranthene		$C_{16}H_{10}$	4	202.25	110.8	375	0.26	1.2×10^{-3}	5.22
Pyrene		$C_{16}H_{10}$	4	202.25	156	393–404	0.13	6.0×10^{-4}	5.18
Benzo[a]anthracene		$C_{20}H_{12}$	4	228.29	158	438	0.011	2.8×10^{-5}	5.91
Chrysene		$C_{18}H_{12}$	4	228.29	254	448	0.006	5.7×10^{-7}	5.91
Benzo[b]fluoranthene		$C_{20}H_{12}$	5	252.31	168.3	No data	0.0015	-	5.80

Table 1. *Cont.*

Compound Name	Chemical Structure	Chemical Formula	Number of Rings	Molecular Weight (g\mol)	Melting Point (°C)	Boiling Point (°C)	Aqueous Solubility (mg/L)	Vapor Pressure (Pa)	Log K_{ow}
Benzo[k]fluoranthene		$C_{20}H_{12}$	5	252.31	215.7	480	0.0008	5.2×10^{-8}	6.00
Benzo[a]pyrene		$C_{20}H_{12}$	5	252.31	179–179.3	495	0.0038	7.0×10^{-7}	5.91
Dibenzo[a,h]anthracene		$C_{22}H_{14}$	6	278.35	262	No data	0.0006	3.7×10^{-10}	6.75
Benzo[ghi]perylene		$C_{22}H_{12}$	6	276.33	273	550	0.00026	1.4×10^{-8}	6.50
Indeno[1,2,3-cd]pyrene		$C_{22}H_{12}$	6	276.33	163.6	530	0.00019	-	6.50

Synthetic organic dyes are introduced in the aquatic environment [74,75] because of their extensive usage in printing, paint, and textile industries. These compounds are characterized especially by their non-reactivity, long-lasting coloring, and highly stable structures [74]. Besides their carcinogenic effect, many dyes affect human life, such as dysfunction of the central nervous system (CNS), kidney, reproductive system, brain, and liver [74,76,77]. Wastewaters from textile and other dyes industrial processes contain large quantities of these organic pollutants, which are difficult to degrade during the standard biological methods and resist aerobic degradation. Moreover, Due to their high solubility in water, the removal of the dyes from wastewater through conventional methods is very difficult and ineffective [71,78]. Degradation of certain types of dye produces more hazardous pollutants than the dye itself. For example, under anaerobic conditions, organic dyes, such as azo dye, can be reduced to potentially carcinogenic aromatic amine [68,79].

3. Methods of Treatment

As outlined beforehand, toxic organic pollutants are widespread in the environment, thus, it is highly recommended to eliminate or reduce the concentration of such pollutants in the aquatic environment to safe levels [53,80–83]. Numerous conventional treatment processes have been applied and tested for wastewater treatment, such as adsorption, coagulation, precipitation, biodegradation, ozonation, electrochemical oxidation, and advanced oxidation processes [43,47,83–88]. Besides that, combining some of these processes, such as the biological–physical, or chemical processes, has been successfully applied in many wastewater treatment plants [89–92]. Although many of these processes have been considered effective and efficient for removing a wide spectrum of organic pollutants from the wastewater; however, each process has disadvantages that limit the large-scale application, e.g., small capacity, high costs, pH-dependency, limited recyclability, high-energy requirements, incomplete pollutant removal, and generation of toxic secondary materials (Table 2) [87,93–96].

Table 2. Different removal techniques used for wastewater treatment and their advantage(s) and disadvantage(s).

Removal Techniques	Advantage(s)	Disadvantage(s)
a) *Coagulation*	• The additive coagulants easily settled with the suspended particle. • Rapid and efficient for insoluble contaminants. • Low-cost operation.	• pH monitoring of the effluent. • The dissolved organic pollutants are not completely removed. • Formation of sludge and secondary pollutants.
b) *Electrochemical oxidation*	• Recycling of valuable metals. • Increases biodegradability. • Not require auxiliary chemicals or high temperatures.	• Required pre-filtration; formation of sludge. • High initial cost of the equipment • Low selectivity and low reaction rates.
c) *Biological process*	• Simple, economically attractive. • Ecologically favorable process.	• Poor decolorization. • Formed uncontrolled degradation products. • High capital and operational cost. • The secondary sludge problems.

Table 2. *Cont.*

Removal Techniques	Advantage(s)	Disadvantage(s)
d) *Adsorption*	• Cost-effective and simple method. • The most profitable process and more efficient than the conventional methods (i.e., precipitation, solvent extraction, membrane filtration, etc.).	• Removes the pollutants from one phase (aqueous) to another (solid matrix). • Expensive regeneration process especially if the pollutants are strongly bound to the adsorbents.
e) *Chemical precipitation*	• Adapted to high pollutant loads. • Simple equipment and processes.	• Chemical consumption. • High sludge production.
f) *Advanced Oxidation Processes (AOP)*		
I. Ozonation	• Powerful oxidation technique for a large number of pollutants.	• Complex technology. • High capital/operational cost. • High electric consumption.
II. UV	• An effective method that typically does not produce harmful by-products.	• Low efficiency when the wastewater contains a high number of particulates that absorb UV light.
III. UV/H_2O_2	• An effective technique in the oxidation and mineralization of most organic pollutants. • Ease formation of OH$^•$ radicals.	• Less effective, when the wastewater has high absorbance. • High operational cost.
IV. O_3/UV/H_2O_2	• Most effective process due to the fast generation of OH$^•$ radicals. • Can treat a wide variety of contaminants.	• Needs to compete with high turbidity, solid particles, and heavy metal ions in the aqueous stream. • High operational cost.
V. Fenton reaction	• Simple process. • Easy availability of chemicals.	• Production of iron sludge waste, bringing logistical problems with handling.
VI. Photo-Fenton reaction	• Reduction of sludge iron waste compared to the original Fenton reaction. • Effective and fast degradation.	• Requires a controlled pH medium for better performance.
VII. Heterogeneous photocatalysis	• Long-term stability at high temperature. • Resistance to attrition. • Low-cost and environmentally benign treatment technology.	• Formation a harmful byproduct to the environment. • Requires efficient catalysts that can absorb a wide range of light.

Among many developed and examined methods for eliminating the persistent organic pollutants from the environment (especially aquatic environment), advanced oxidation processes (AOPs) are the most promising techniques. They are also the most studied and the best environmental-friendly techniques for removing these pollutants. These processes are based on the formation of in-situ highly reductive or oxidative free radicals, e.g., hydroxyl radicals (OH$^•$), at sufficient concentration to effectively mineralize the hazardous organic

compounds and decontaminate water under ambient conditions [95,97]. Several AOP techniques have been explored to decompose the organic pollutants in the water resources by chemical oxidation or reduction such as ozonation, H_2O_2 photolysis, Fenton process, photo-Fenton process, and heterogeneous photocatalysis [97–100]. Scheme 1 shows the types and the general classification of the AOP [100].
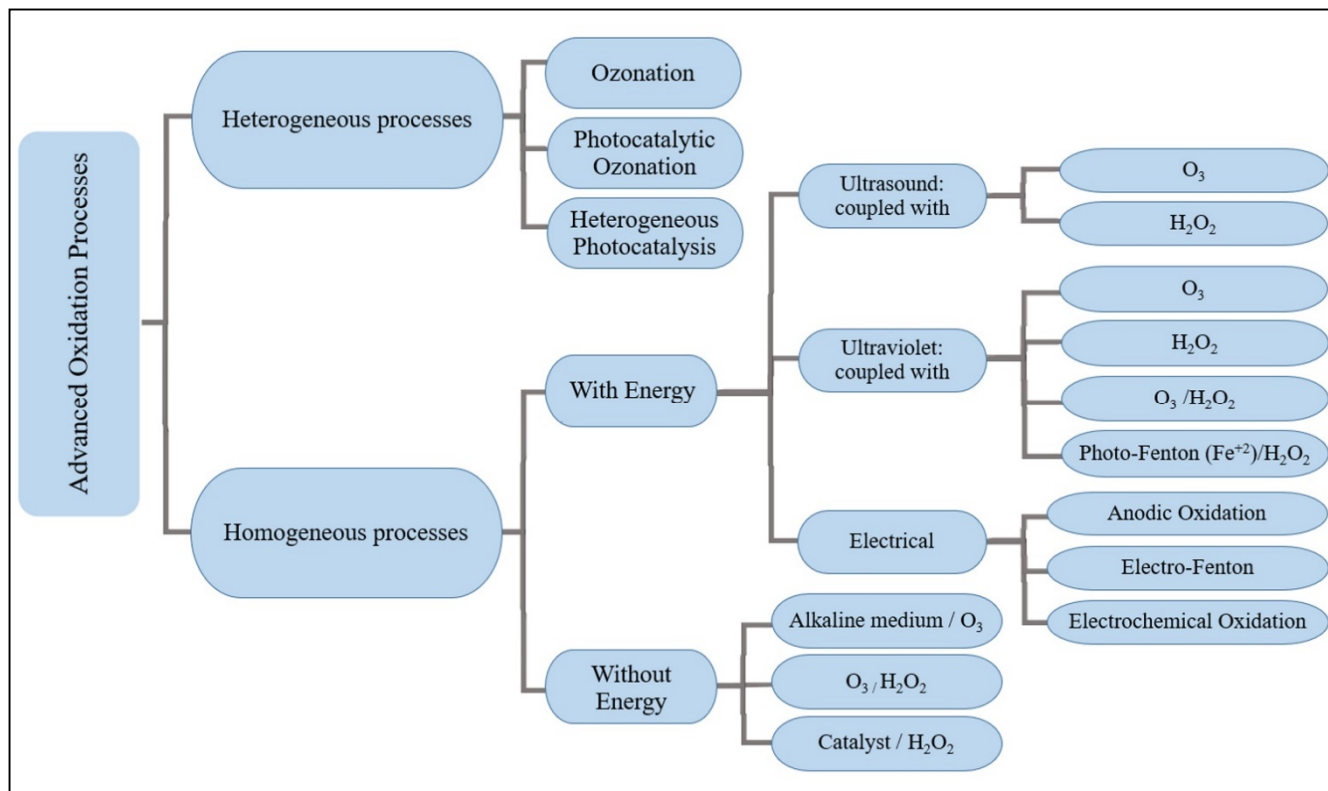
Scheme 1. General classification of the AOP. Adapted from reference [100].

By far, heterogeneous photocatalysis has gained the most attention as one of the most realistic and viable solutions due to its ability to clean-up a wide range of environmental pollutants besides the use of low-cost and chemical stable photocatalysts [101–108]. This promising approach relies on the excitation of a semiconductor with suitable light, e.g., the sunlight, to drive different redox reactions. Heterogeneous photocatalysis is a process that includes a large variety of reactions, such as oxidation, dehydrogenation, water splitting (reduction, H_2 production; oxidation, O_2 production), organic synthesis, photoreduction, metal deposition, hydrogen production, gaseous pollutant removal, and water purification [109]. Photocatalysis is a sustainable and economical technology that can exploit the inexhaustibly abundant clean energy of the sun [104,109,110]. The use of an efficient nanoparticulate semiconductor is required for the detoxification of the wastewater via photocatalysis, which has the potential to degrade the toxic substances in the water, such as contaminants and microorganisms [111–113]. Due to their narrow bandgap and distinct electronic structure (unoccupied conduction band and occupied valence band) [20,114,115], various kinds of photocatalysts, including TiO_2, Gr-TiO_2, CdS, SnO_2, WO_3, SiO_2, ZnO, Nb_2O_3, Fe_2O_3, have been studied to degrade a variety of organic and inorganic pollutants [102,115–117].

Nowadays, the photooxidation of organic pollutants based on TiO_2 nanomaterials is still gain huge attention. Several recent studies have shown the effective role of TiO_2 in oxidizing and mineralizing a wide range of hazardous organic contaminants [118,119], such as alcohol [120,121], organic acids [122], aromatic hydrocarbons [104], phenols [123], dyes [124], pharmaceuticals [125,126], and pesticides [126]. The photocatalytic oxidation

of organic pollutants proceeds either by the direct attack of the photogenerated holes or via the attack of the highly reactive hydroxyl radicals generated at the surface of the photocatalyst [110]. The photocatalytically generated OH$^\bullet$ radicals can abstract hydrogen atoms from the organic molecules, causing a chain of reactions toward lower molecular intermediates and may end up in the complete mineralization of the pollutants [127].

Another major field in photocatalysis includes light-driven water splitting into H_2 and O_2 [128]. H_2 is regarded as the most recommended replacement for fossil fuels since its energy cycle is free of pollutants and greenhouse gases [105,129,130]. Achieving dual-functional photocatalysis, i.e., the photocatalytic degradation of organic pollutants and the simultaneous production of hydrogen gas is an added value of this technique [131]. Unfortunately, as will be discussed in the following sections, different operational conditions should be applied for each process to achieve its optimal reaction yield [11].

4. Semiconductor-Based Heterogeneous Photocatalysis

A photocatalytic system is thermodynamically defined as a system, in which a reaction with $\Delta G < 0$ is driven through the photon absorption by a suitable material, i.e., the light energy is exploited to drive a reaction having extremely low kinetics outside this system [132]. The photons are absorbed by such a system to generate accordingly charge carriers, i.e., electrons and holes, which induce a redox reaction. The semiconductors could be the light-absorbing materials in heterogeneous systems and they are then known as photocatalysts [133]. Thus, heterogeneous photocatalysis depend on the distinctive properties of powdered semiconductor materials in harvesting incident light, generating charge carriers, and subsequently initiating surface reactions. This may provide a simple means for environmental remediation and photochemical energy conversion into fuels [134,135].

4.1. The Electronic Structure of a Semiconductor–Photocatalyst

The band model based on the concept of molecular orbitals can be used to explain the electronic structure of a semiconductor. The electronic orbitals merge and split into two bands, i.e., the valence band (VB) and the conduction band (CB). VB and CB of a semiconductor are formed from the highest occupied molecular orbitals (HOMO) and the lowest unoccupied molecular orbitals (LUMO), respectively [136]. At temperature 0 K, the VB is the lower band that is completely filled with electrons, while the CB is the higher band that is empty [137]. The difference in energy between the highest energy level in the VB and the lowest energy level in the CB creates a region known as the energy bandgap (E_g) [138]. The interaction between the electronic orbitals, forming the band structure of a semiconductor is shown in Figure 2. Interestingly, the E_g values for semiconductors are sufficiently small that the electrons promotion from the VB to the CB can be initiated through an energy transfer to those materials [132]. The light energy that is higher or equal to E_g induces the excitation of electrons from the VB to occupy partially filled states in the CB generating an electron vacancy in the VB, which is known as the positively charged hole [139]. This hole is considered as a mobile entity since it can be filled by another electron creating a vacancy in the space where it has been transferred from [140]. The electrons in the CB are, likewise, mobile entities having often higher mobility than those of the holes (e.g., for Si, $\mu_{n(electrons)} = 1500 \, cm^2 \cdot V^{-1} \cdot s^{-1} > \mu_{p(holes)} = 450 \, cm^2 \cdot V^{-1} \cdot s^{-1}$ [141]). Electrons have consequently a higher diffusion coefficient than holes; however, the trapping of the electrons leads to a decrease in their mobilities [142]. The e^-/h^+ species migrate then to the surface of the semiconductor, where they can react with the adsorbed molecules. The photogenerated holes act as oxidants (+1.0 to +3.5 V vs. NHE), while the photogenerated electrons are potential reductants (+0.5 to −1.5 V vs. NHE) [143].
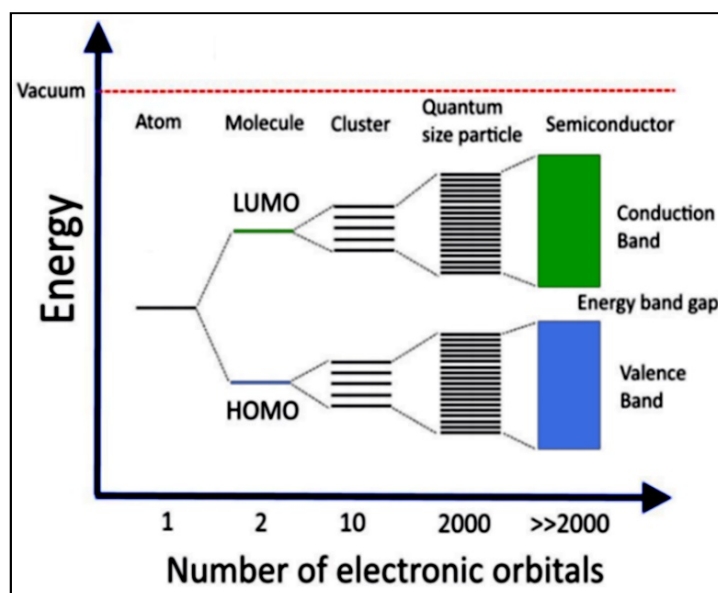
Figure 2. Band structure of a semiconductor as an interaction of atomic orbitals. adapted from reference [144]. Copyright 1997 Elsevier B.V.

Semiconductor photocatalysis is considered, from this point of view, as a multi-step process, which is illustrated in Figure 3. Such a process is initiated by the photoexcitation with electromagnetic radiation equal to or exceeding E_g (1), the separation of the charge carrier pairs (2), the diffusion of e^-/h^+ species within the material towards the surface, and the surface charge transfer for the reduction of adsorbed electron acceptors (3), and the oxidation of adsorbed electron donors (4), respectively [145,146]. Accordingly, the photo-induced electrons and holes should migrate to reach the surface of the material and react with adsorbed chemical species via surface charge transfer [144]. Therefore, the E_g of a semiconductor is the minimum thermodynamic requirement for photocatalysis [147–149].
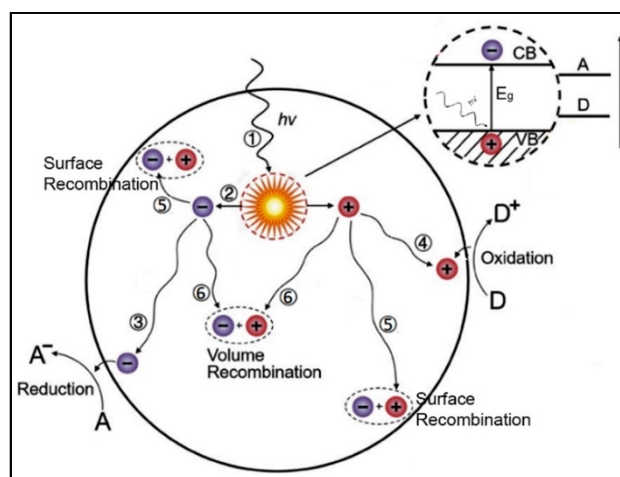
Figure 3. Pathways of the photogenerated charge carriers in a semiconductor photocatalyst. Adapted with permission from reference [149]. Copyright 2013 John Wiley and Sons.

One of the main limitations of semiconductor photocatalysis is the recombination of the photogenerated charge carriers, dissipating the absorbed energy as heat [138] and affecting negatively the lifetime of the electrons and holes [144]. This undesired recombination occurred either indirectly, i.e., via surface defects (5), or directly, i.e., by band-to-band recombination (6). Such phenomena are highly reliant on the crystal structure of the semiconductor. To enhance effectively the redox reactions while minimizing recombination, the

photogenerated charge carriers must migrate to the liquid junction through the solid and should react with adsorbed species directly at the semiconductor surface [148].

4.2. Photocatalytic Water Splitting vs. Photocatalytic Reforming

Photocatalytic H_2 production from water splitting is accomplished under ambient operating conditions and consists of two half-reactions as shown in Equations (1) and (2), i.e., the reduction of proton and the 4-electron oxidation of water, respectively [150]. A change in free energy of $\Delta G^0 = 237.2$ kJ mol^{-1} is associated with the splitting of one H_2O molecule to H_2 and ½ O_2, which equals to $\Delta E° = 1.23$ V according to the Nernst equation [151]. Thus, the semiconductor should absorb photon energy of more than 1.23 eV (wavelengths shorter than 1000 nm) to drive the water splitting photoreaction. The semiconductor can use their photogenerated electrons/holes to convert the photon energy into H_2 and O_2 when the energy of the conduction band-edge and the valence band-edge straddle the electrochemical potentials $E°$ (H$^+$/H$_2$) and $E°$ (O$_2$/H$_2$O), respectively [150,152] (Figure 4). Accordingly, the thermodynamic requirement for the water splitting is more cathodic and more anodic energy levels of the CB bottom and VB top of a photocatalyst compared to the standard electrode potential of (H$^+$/H$_2$) and (O$_2$/H$_2$O), respectively [152,153]. Therefore, from a thermodynamic point of view, only a few photocatalysts, e.g., TiO_2, are proficient to drive the water splitting reaction. However, the efficiencies of heterogeneous photocatalytic water splitting remain relatively low due to many reasons outlined in the next sections.

$$2H^+ + 2e^- \rightarrow H_2 (\uparrow) \qquad E^0 = 0 \text{ V } vs. \text{ NHE} \qquad (1)$$

$$H_2O \rightarrow \frac{1}{2}O_2 (\uparrow) + 2H^+ + 2e^- \qquad E^0 = 1.23 \text{ V } vs. \text{ NHE} \qquad (2)$$
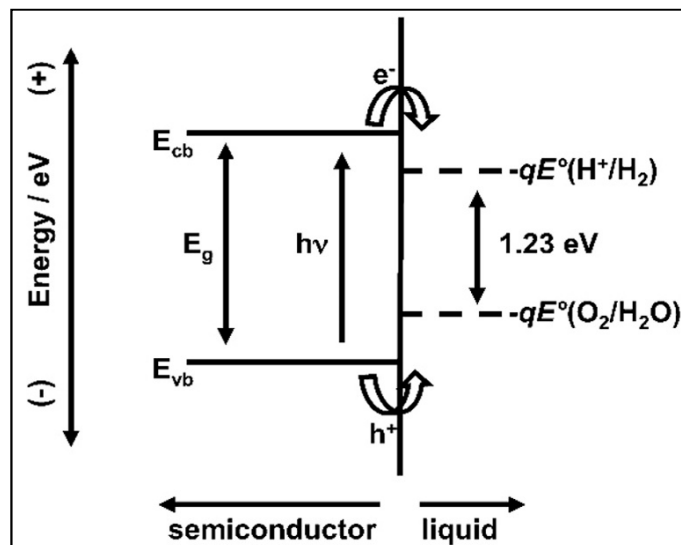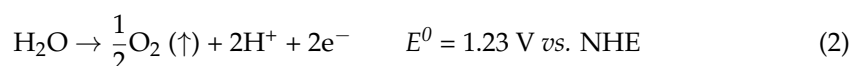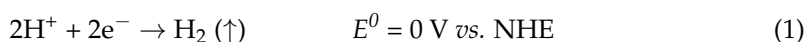
Figure 4. Photocatalytic water splitting at the surface of an irradiated semiconductor, reprinted from reference [152]. Copyright 2010 American Chemical Society.

As a hybrid field, dual-functional photocatalysis is a combination of different photocatalytic fields for 2-fold purposes achieved in a single step [130]. The coupling of H_2 evolution and photocatalytic degradation of organic pollutants yielding CO_2 can be achieved in the so-called photoreforming process [38,132,153–156]. Such a technique has a great advantage as it can benefit from solar light to treat wastewater, meanwhile, the evolved CO_2 can be consumed by natural photosynthesis [157]. In the photocatalytic reforming process, the photogenerated holes in the valence band can oxidize adsorbed organic substrates (electron donors or sacrificial reagents), whereas the photogenerated electrons in the conduction band can reduce the protons (electron acceptor) to molecular hydro-

gen [104,105,130,158,159]. Such an adsorbed organic substrate can react irreversibly with the photogenerated holes, minimizing the undesired electron/hole recombination [150].

Even though H_2 can be formed simultaneously with other processes, e.g., the organic synthesis of organic compounds [160,161], however, such processes should not be considered as a dual function process [130]. The reforming process can be considered as a dual function photocatalysis process only when some requirements have been met: (i) H_2 is mainly derived from the reduction of water and (ii) the targeted organic molecules are pollutants, or their oxidation aimed to synthesize value-added products, such as aldehyde, organic acid, and imine [130,162]. Consequently, photocatalytic reforming is an intermediate process between photocatalytic water splitting and the photocatalytic oxidation of organic pollutants as shown in Figure 5.
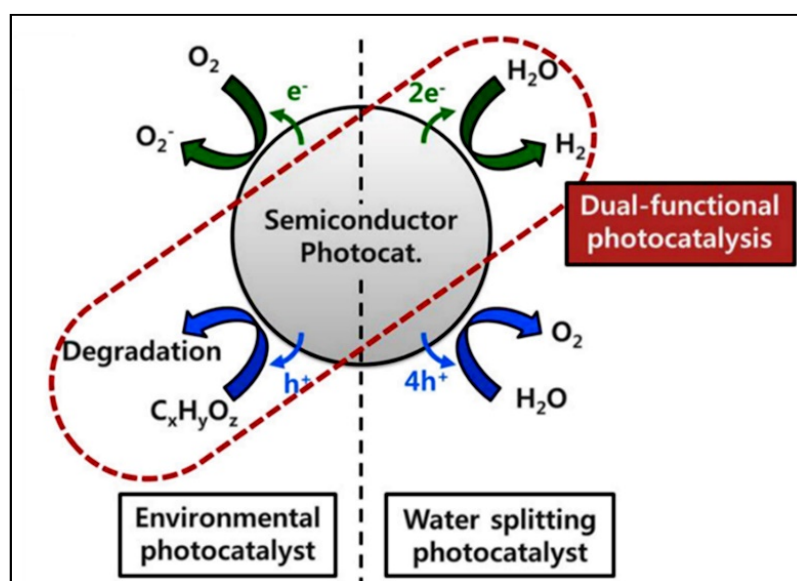
Figure 5. Dual-function photocatalysis process. Reprinted with permission from reference [158]. Copyright 2018 American Chemical Society.

Organic substrates are generally stronger reducing agents than water, hence, a less positive potential is necessary to oxidize these compounds. Accordingly, the energetic separation of the redox half-reactions in photoreforming is narrower compared to that of the overall water splitting [163]. As O_2 is not produced in these systems, the back reaction to produce water is suppressed, avoiding a subsequent gas separation stage [164]. A wide range of organic compounds such as alcohols, organic acids, and hydrocarbons had proven activity as electron donors for photocatalytic H_2 production [101,104,105,131,150,165–167]. The evolution of H_2 and its kinetic reactions pathway is dependent on the concentration and the nature of the organic substrate [168,169].

4.3. Titanium Dioxide (TiO_2) as a Photocatalyst

Titanium dioxide has been one of the most widely studied semiconductors in the last decade for various photocatalytic applications [170]. This is related to its high reactivity, hydrophilicity, low cost, and availability, physical and chemical stability, resistance to photocorrosion, and optimal electronic and optical capacity [97,111,139]. TiO_2 is a transition-metal oxide semiconductor composed of Ti^{4+} atoms and six O^{2-} coordinated together to form a TiO_6 octahedron [171]. Like other transition metal oxides, TiO_2 is often nonstoichiometric with oxygen vacancies (O_v) as predominant defects at the near-atmospheric oxygen pressure, granting it the properties of an intrinsic n-type semiconductor [172]. The oxygen vacancies (O_v) at the surface of n-type TiO_2 appear as extra unpaired electrons in the CB [164,173], which act as donor-like states. This creates an accumulation layer in the surface, resulting in a downward band bending [174].

The photocatalytic activity of TiO_2 is highly related to its charge carrier dynamics. The e^-/h^+ pairs are generated within a few femtoseconds upon irradiation and they can recombine easily either in the bulk or at the surface. However, other charge carriers escape recombination and migrate to the surface, where they might be trapped before the interfacial charge transfer in redox reactions [175]. Figure 6a and Equations (3)–(6) demonstrate the potential fates of charge carriers upon the irradiation of TiO_2, while Figure 6b reports the time scale of each process [143,176].
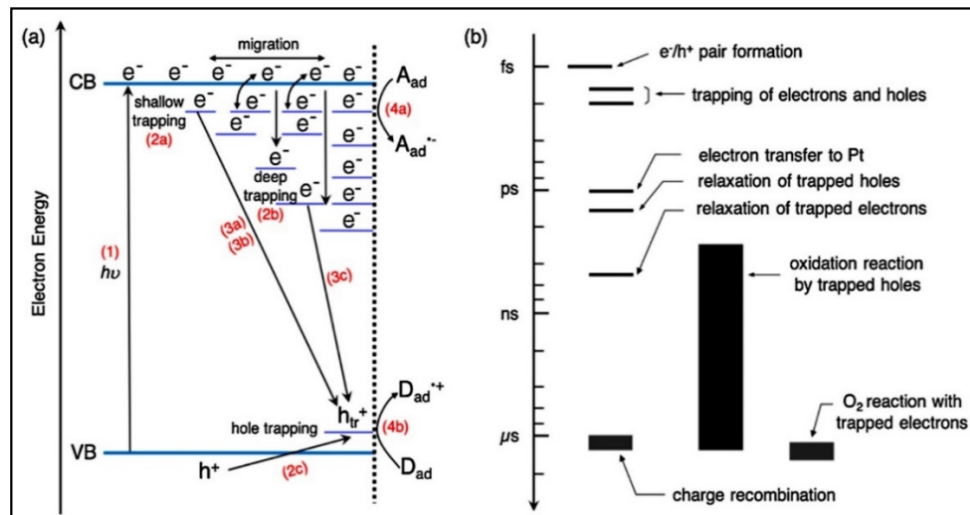
Figure 6. The possible charge carrier pathways on irradiated TiO_2. (**a**) The possible charge carrier pathways on irradiated TiO_2 and (**b**) the time scale after irradiation for each pathway. Reprinted with permission from reference [175]. Copyright 2019 Elsevier B.V.

Photogeneration of the charge carriers:

$$TiO_2 + hv \rightarrow TiO_2 \; (e^-_{CB}/h^+_{VB}) \tag{3}$$
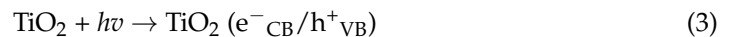
Trapping of the charge carriers:

$$e^-_{CB} + \equiv Ti^{IV}OH \rightarrow \equiv Ti^{III}OH \; \text{(shallow trapping)} \tag{4a}$$

$$e^-_{CB} + \equiv Ti^{IV} \rightarrow \equiv Ti^{III} \; \text{(deep trapping)} \tag{4b}$$

$$h_{VB}^+ + \equiv Ti^{IV}OH \rightarrow \{Ti^{IV}OH^\bullet\}^+ + (h^+_{tr}) \tag{4c}$$

Recombination of the charge carriers:

$$e^-_{CB} + \{Ti^{IV}OH^\bullet\}^+ \rightarrow Ti^{IV}OH \tag{5a}$$

$$h+_{tr} + \equiv Ti^{III}OH \rightarrow Ti^{IV}OH \tag{5b}$$

$$h^+_{tr} + Ti^{III} \rightarrow Ti^{IV} \tag{5c}$$
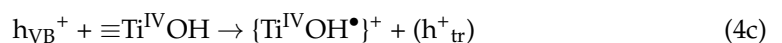
Interfacial charge transfer to the acceptor (A) or donor (D) adsorbed on the surface:

$$\equiv Ti^{III}OH + A \rightarrow \equiv Ti^{IV}OH + A^{\bullet-} \tag{6a}$$

$$\{Ti^{IV}OH^\bullet\}^+ + D \rightarrow \equiv Ti^{IV}OH + D^{\bullet+} \tag{6b}$$
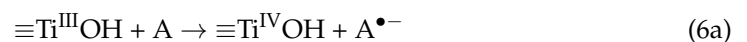
Serpone et al. found that in the absence of scavengers, more than 90% of the initially formed charge carriers recombine rapidly within 10 ns upon the irradiation of TiO_2 in aqueous media. Such high recombination results in less than 10% quantum yields of photooxidation [177].

On the other hand, the photogenerated charge carriers can be trapped either in the bulk or at the surface as trapped holes and trapped electrons, with the surface trapping being preferred for the subsequent interfacial charge transfer reactions [178]. Yoshihara et al. showed in their Transient Absorption Spectroscopy study that both trapped holes and electrons are found to be localized at the surface of photoexcited TiO_2 particles, while free electrons are distributed in the bulk [179]. Howe and Gratzel demonstrated in their Electron Paramagnetic Resonance spectroscopy (EPR) studies on irradiated TiO_2 that the photogenerated electrons are localized in the d orbitals of Ti^{4+} while the photogenerated holes are trapped at the lattice oxygen atoms, forming EPR-active paramagnetic centers, i.e., Ti^{3+} and $O^{\bullet-}$, respectively [180,181]. Simultaneously, upon the generation, separation, and transport of charge carriers in TiO_2, e^-/h^+ pairs might participate in redox reactions *via* interfacial charge carrier transfer. In aqueous media, water layers adsorb, physically and chemically, on the TiO_2 surface creating a TiO_2/H_2O interface [182]. The photogenerated holes can react on the surface either with hydroxyl groups or with H_2O resulting in the formation of hydroxyl radicals, $OH^{\bullet}$. Therefore, not only h^+ is produced by the photoexcitation of TiO_2 but also hydroxyl radicals can be formed on hydrated TiO_2 surfaces.

TiO_2 has three main crystal phases: anatase, rutile, and brookite. While anatase and rutile exhibit the same tetragonal crystal structures, brookite has an orthorhombic crystal structure. These three polymorphs have also different E_g values, i.e., 3.2 eV, 3.0 eV, and 3.3 eV for anatase, rutile, and brookite, respectively [30]. Anatase has been generally considered as the most active phase of the three TiO_2 polymorphs for photocatalytic applications [183,184].

Anatase and rutile TiO_2 have shown differences in their respective charge carrier recombination kinetics [185,186]. Using transient absorption spectroscopy, Sachs et al. [185] compare the ultrafast charge carrier kinetics for anatase and rutile in dense and nanostructured TiO_2 films. They found that bulk rather than surface recombination was the key determinant of charge carrier lifetime. They also monitored that recombination was dependent on the crystal phase. Rutile shows faster recombination than anatase, which is consistent with the doping density (n-type doping due to oxygen vacancies) in rutile being higher than in anatase. Besides, Wang et al. [187] investigated anatase and rutile TiO_2 with photoluminescence spectroscopy under weak excitation conditions. Anatase showed a visible emission, while a NIR emission was reported in rutile; however, both emission spectra exhibited long lifetimes up to milliseconds. They explained that the NIR luminescence band in rutile TiO_2 was due to the recombination of trapped electrons with free holes. Hence, trap states in TiO_2 may play a very important role in the photocatalysis processes. The depth of trap states in rutile TiO_2 is much deeper than that in anatase TiO_2, which has shallowed-trapped electrons in addition to a higher number of free electrons as shown in Figure 7a,b. On the other hand, Durrant et al. [188] employed transient absorption spectroscopy (TAS) to investigate the kinetic of photocatalysis in anatase and rutile TiO_2 films. Although rutile exhibited 10 times slower recombination kinetics than anatase, mesoporous anatase film was around 30 times more efficient than mesoporous rutile film in the photocatalysis of the "intelligent ink" model system. They found also that in the presence of alcohols, faster and irreversible hole scavenging was achieved on anatase than in the case of rutile, resulting in the creation of long-lived electrons ($\tau \approx 0.7$ s). The authors explained the lower activity of rutile to the deficiency of rutile holes to drive efficient and irreversible alcohol oxidation rather than to the differences in recombination kinetics.

Figure 7. Tapping and recombination of photogenerated charge carriers in anatase (**a**) and rutile (**b**), reprinted with permission from reference [175]. Copyright 2019 Elsevier B.V.

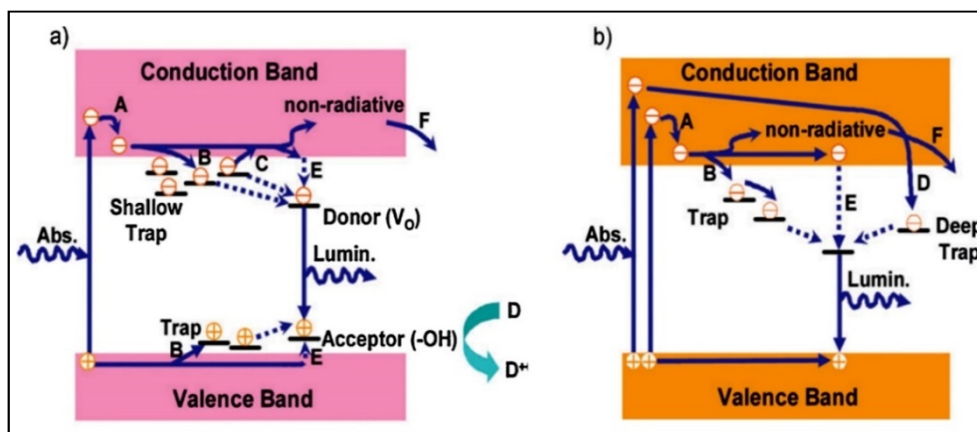Choi et al. [189] compared the recombination kinetics in anatase and rutile using time-resolved diffuse reflectance (TDR) spectroscopy. They demonstrated that during the 355 nm laser excitation, the time-resolved decay at 550 nm was slower in anatase than rutile as shown in Figure 8a. This results in a longer lifetime of photogenerated charge carriers with subsequent higher reactive oxygen species generation in anatase. The authors observed also the generation and the diffusion of OH$^\bullet$ from the illuminated TiO$_2$ surface to the solution bulk using a single-molecule detection method. They found that only anatase generates mobile OH$^\bullet$ radicals, therefore, the photocatalytic oxidation on rutile is limited to adsorbed species. Schindler and Kunst [190] studied the excess charge carrier kinetics in anatase and rutile TiO$_2$ powders using the time-resolved microwave conductivity (TRMC) method. Figure 8b shows the transient change of the reflected microwave power after excitation by a 20-ns laser pulse at 266 nm. The photoconductivity in anatase decays very slowly compared to rutile powder. They demonstrated that this signal can be attributed to excess electrons in the CB because of the n-doping characteristics and the larger electron mobility compared to the hole mobility. Therefore, the short electron lifetime in rutile could be due to a higher recombination rate, while in anatase fast trapping of the minority charge carriers (holes) may take place. This would decrease the availability of holes for recombination and reduce the recombination probability, leading to a longer lifetime in anatase.
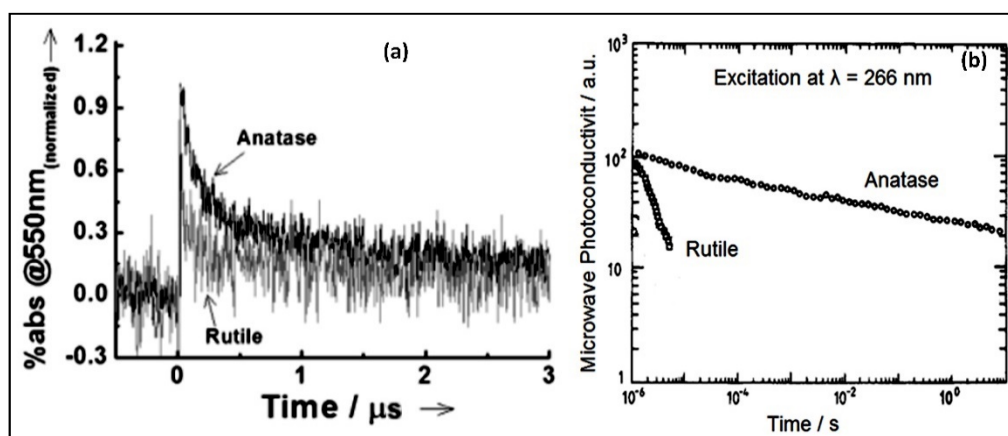
Figure 8. (**a**) Time-resolved diffuse reflectance spectroscopy measurements with normalized absorbance at 550 nm during the 355 nm laser excitation (1.5 mJ pulse^{-1}) of aqueous suspensions of anatase and rutile TiO$_2$ in water. Adapted with permission from reference [189]. Copyright 2013 John Wiley and Sons. (**b**) Photoconductivity of TiO$_2$ powders after a laser flash excitation at 266 nm with energies of 0.5 and 1 mJ cm^{-2} for anatase and rutile, respectively. Adapted with permission from reference [190]. Copyright 1990 American Chemical Society.

The development of TiO$_2$ materials has led to mixed-phase titania photocatalysts. One example is P25-TiO$_2$, which is a mixture of anatase and rutile (75:25). Due to its higher activity, anatase is conventionally considered to be the active component in P25, with rutile serving as an electron sink. Some reports showed that such mixed-phase titania has slower rates of charge carrier recombination, higher photo-efficiencies, and lower energy light activation [191]. Knorr et al. [186] studied the room-temperature photoluminescence spectra of nanocrystalline TiO$_2$ in the anatase and rutile phases and mixed-phase films. They showed that the photoluminescence of anatase results from at least two spatially isolated trap-state distributions, i.e., trapped electrons and trapped holes, which are, respectively, about 0.7−1.6 eV and 1.8−2.5 eV below the conduction band edge. The signal of trapped electrons was largely quenched in P25 and the presence of hole scavengers. The authors, hence, concluded a bidirectional electron transport between anatase and rutile phases in P25, with solvents having a strong impact on the competition for electrons between the two phases.

Additional recombination or trapping in the rutile part decreases the lifetime of electrons compared to pure anatase, but it would be much longer than in pure rutile due to the deep trapping of the holes in the anatase part. On the other hand, Hurum et al. [191] studied the charge separation characteristics of P25 by EPR spectroscopy. They showed, as presented in Figure 9, that the visible light irradiation of rutile produced charge carriers, which are stabilized through electron transfer to lower energetic trapping sites in the lattice of anatase. The authors suggested that the morphology of nanoclusters P25 consists of small rutile crystallites interwoven with anatase crystallites. The transition points between these two phases permit a rapid electron transfer from rutile to anatase. Hence, rutile in P25 acts as an antenna to extend the photoactivity into visible wavelengths and the structural arrangement creates catalytic "hot spots" at the rutile−anatase interface.
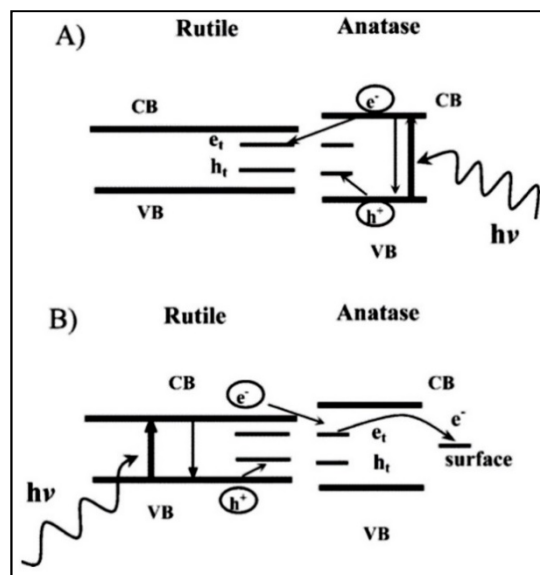
Figure 9. (**A**) Conventional model of P25 activity where charge separation occurs on anatase while rutile acts as electrons sink. (**B**) Proposed model of a rutile antenna and subsequent charge separation. Reprinted with permission from reference [191]. Copyright 1990 American Chemical Society.

Using the time-resolved microwave conductivity (TRMC) method, Schindler and Kunst [190] found that the transient photoconductivity in P25 was rather more like the decay behavior observed in anatase than that in rutile shown in Figure 8b. They expected that in the mixed powder, fast recombination, such as in rutile for the electron–hole pairs created in the rutile part. Nevertheless, the deep trapping of holes in the anatase part would prevent the transfer of holes to the rutile part for the electron–hole pairs created in the anatase part.

4.4. Enhancing the Performance of Pristine TiO_2

As discussed above, although pristine TiO_2 exhibits advantages, some limitations are also presented. The main drawbacks to using pristine TiO_2 as an active photocatalyst are the lack of visible light activation, the fast recombination of the photogenerated electrons and holes, the relatively low charge carrier mobility.

Various attempts have been made to improve the capability to exploit visible photons for the TiO_2 photocatalytic process. Doping with transition metal ions is one approach that has been extensively employed, especially the incorporation of Fe^{3+} into the TiO_2 matrix [164]. This has been proven as a promising method to create additional states in the bandgap and, consequently, to an increase in the absorption of the visible light [102]. Moreover, it can introduce electron capture centers, resulting in a decrease in electron/hole recombination centers [164]. Compared to pristine TiO_2, Fe-doped TiO_2 has enhanced light-harvesting; however, controversial results on its photocatalytic activity have been reported [102]. Choi et al. [192] studied the photocatalytic oxidation of chloroform using TiO_2 doped with 21 transition metal ions and discovered that the doping with Fe^{3+}, Mo^{5+}, Ru^{3+}, Os^{3+}, Re^{5+}, V^{4+}, and Rn^{3+} cations is beneficial. Moreover, nonmetal doping has been widely studied, especially with N, C, F, B, and other elements having an atomic radius similar to that of the O atom. Among them, nitrogen has attracted much attention. Asahi et al. [193], for example, showed that nitrogen-doped TiO_2 exhibits enhanced visible light absorption and photocatalytic activity. Other strategies are the use of noble metals (e.g., Pt, Au, Pd, Rh, Ni, Cu, and Ag) as a co-catalyst to decrease the recombination of the charge carriers and provide additional active sites for H_2 evolution [102]. We will focus in the next sections on the modification of pristine TiO_2 with noble-metal co-catalysts, particularly platinum nanoparticles, due to their higher catalytic performance driving the reduction reaction of protons [104]; hence, increasing the photocatalytic reforming of organic compounds.

The energy of the photogenerated electrons in the conduction band for both rutile (E_{CB} = −0.11 V at pH 0) and anatase (E_{CB} = −0.32 V at pH 0) [145] is sufficient to form H_2 by reducing water. However, pristine TiO_2 has been reported as an inactive photocatalyst for H_2 production because of the fast recombination of charge carriers and the inability to reduce protons to H_2 due to the higher overpotential for hydrogen evolution reaction (0.05 V) [194]. Hence, even in the presence of an electron donor, pristine TiO_2 has shown an inability to catalyze the hydrogen evolution reaction [131]. TAS data revealed that the generated electrons are trapped as blue Ti^{3+} ions instead of reducing H^+ upon the consumption of holes by the electron donor [105,195]. Consequently, it is highly recommended to modify pristine TiO_2 with an appropriate co-catalyst, which can effectively catalyze the cathodic H_2 evolution reaction. One successful strategy is the surface modification with noble metal nanoparticles, e.g., Pt and Au NPs. Noble-metal-modified TiO_2 photocatalysts have been widely studied in the literature, in which the noble-metal NPs act as Hydrogen Evolution Reaction (HER) catalysts.

HER on metallic platinum, as an example, induce via the Volmer reaction, in which $H^\bullet_{ads}$ atoms are produced when the accumulated electrons in Pt are transferred to the proton adsorbed H^+_{ads} and H_2O_{ads}, respectively, as described in Equations (7a) and (7b) [196]. The reaction proceeds afterward through two possible pathways, either the Heyrovsky reaction (Equation (7c)) or the Tafel reaction (Equation (7d)), in which $H^\bullet_{ads}$ react with H^+_{ads} or/and the direct recombination of two $H^\bullet_{ads}$ with each other, respectively [155]. Figure 10 illustrates the two-electron transfer reaction that occurs on the metal surface in acidic solutions. HER on Pt has been shown to exhibit pseudo-first-order kinetics, which indicates that the rate-determining step of the HER is the Volmer reaction [197]. Rabani et al. [197] have presented a linear increase in e^-_{TiO2} decay rate while increasing H^+ concentration at a given Pt concentration, suggesting that H_2 is most likely generated by reduction

of H+ rather than the reduction of H$_2$O. They have also highlighted that the presence of Pt is vital for reactions **7a** and **7b** to occur.
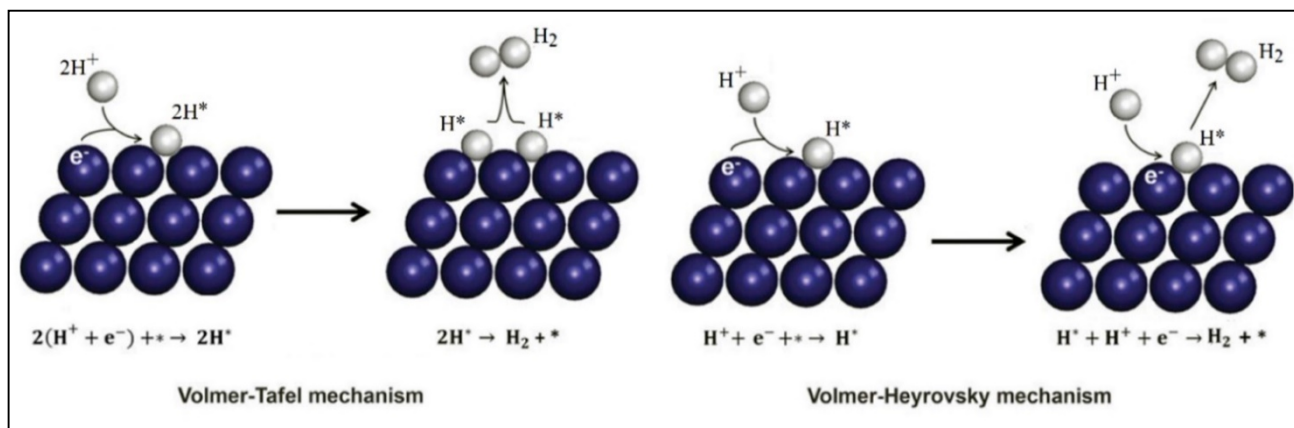
$$H+ads (Pt) + e-(Pt) \rightarrow H\bullet ads (Pt) \qquad (7a)$$

$$H2Oads(Pt) + e-(Pt) \rightarrow H\bullet ads (Pt) + OH- \qquad (7b)$$

$$H\bullet ads (Pt) + e-(Pt) + H+ads (Pt) + e-(Pt) \rightarrow H2(g) \qquad (7c)$$

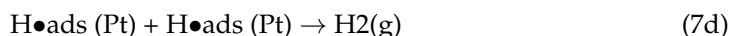$$H\bullet ads (Pt) + H\bullet ads (Pt) \rightarrow H2(g) \qquad (7d)$$
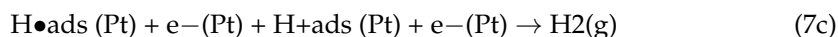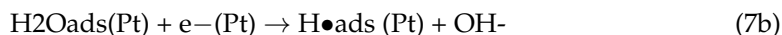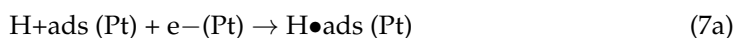

Figure 10. The possible mechanisms of HER on the catalyst surface in acidic solutions. The (*) refers to the active sites of the catalyst, H* refers to the adsorbed H$\bullet$ atom at the active site of the catalyst. Reprinted with permission from reference [198].

It has been widely accepted that enhancement of the activity through the modification of TiO$_2$ with noble-metal NP$_S$ is due to a better charge separation according to the Schottky barrier model. Noble-metal NPs have higher Fermi level energy, i.e., 5.65 eV and 5.10 eV for Pt and Au, respectively [199] compared to that of TiO$_2$, i.e., 4.2 eV [200]. Therefore, photogenerated electrons can transfer from TiO$_2$ to the metal NPs through the interface until a thermodynamic equilibrium is achieved [110] as shown in Figure 11a–d. Schottky barrier ΦB is defined as the barrier against the flow of electrons from the metal to the n-type semiconductor, i.e., TiO$_2$ [201]. During the irradiation, this thermodynamic equilibrium will be unsettled, permitting the photogenerated electrons to continuously flow from the CB of TiO$_2$ to the metal NPs [110,202]. It has been generally recognized that such a Schottky barrier smooths electron trapping by the metal, providing better charge separation. The trapped electrons have, therefore, a longer lifetime to promote the reduction reactions [203,204]. Correlations between photocatalytic H$_2$ evolution rates and metal work functions have been thoroughly established [105,205,206]. However, EPR experiments for irradiated Pt/TiO$_2$ revealed simultaneously signals for the Ti^{3+} centers, which confirms that the photogenerated electrons are not transferred completely to the Pt NPs, rather a certain number of them are trapped as Ti^{3+} ions in TiO$_2$ [105,110,181].

Scavenging the photogenerated electrons from TiO$_2$ by the noble-metal NPs is essential but is not the only factor that enhances the HER. According to the Sabatier principle [207], an ideal catalyst for (HER) is characterized by its optimal binding energy with adsorbed atomic hydrogen (H$^\bullet_{ads}$). This binding energy should be neither too strong nor too weak. On the one hand, the active sites for the HER reaction can be blocked and the desorption of H$_2$ becomes the rate-limiting reaction in the case of a strong binding. On the other hand, proton reduction is rate-limiting in the case of weak binding energy with H$^\bullet_{ads}$ [208]. Consequently, a volcano-type dependence between HER rates and metal-H$^\bullet_{ads}$ bond strength has been proposed [209], in which platinum provides the best activity to drive the HER as shown in Figure 12. In conclusion, Pt/TiO$_2$ has been demonstrated to exhibit the highest photocatalytic activity towards H$_2$ production compared to other metal-loaded

TiO$_2$ [105,155,210], such as Au/TiO$_2$. This has been explained by the highest work function of Pt that enhances electrons "sinking" properties, the lowest overpotential for H$_2$ formation, and the optimal binding energy adsorbing atomic hydrogen.
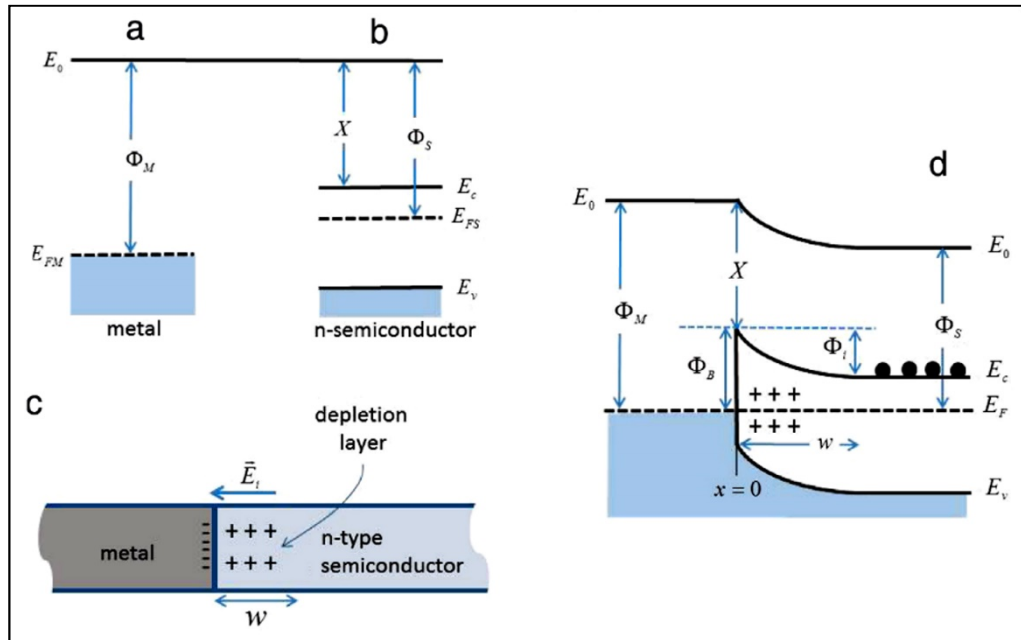
Figure 11. A Schottky barrier formed by a metal of higher work function contacting an n-type semiconductor. (**a**) Metal work function Φ_M and Fermi energy E_{FM}. (**b**) Semiconductor work function Φ_S, electron affinity X and band structure with a bandgap between E_c and E_v and Fermi energy E_{FS}. (**c**) Charge at the metal/semiconductor (M/S) junction. (**d**) Idealized equilibrium band diagram for the M/S junction. Φ_i is the energy barrier to the flow of electrons (black dots) from the semiconductor to the metal, while Φ_B is the Schottky barrier height for the electron flow in the opposite direction. W is the extension of the depletion layer. Reprinted with permission from reference [201]. Copyright 2015 Elsevier B.V.
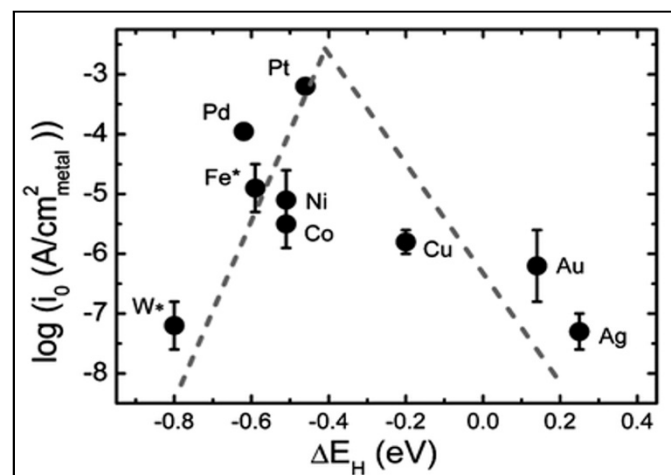
Figure 12. Exchange current densities, log(i$_0$), on monometallic surfaces plotted as a function of the calculated hydrogen binding energy. The data calculated electrochemically for polycrystalline metal disks with a diameter of 5 mm. (*) The data reported for Fe and W were based on the geometric disk area (5 mm in diameter) due to the difficulty in measuring their real surface areas. Reprinted with permission from reference [211]. Copyright 2013 from the Royal Society of Chemistry.

4.5. Effect of the Loading Method on H$_2$ Production

As discussed in Section 4.4, surface decoration of metal (e.g., Au, Ag, Cu, and especially Pt) on TiO$_2$ nanoparticles is an outstanding technique to revamp the electronic properties of TiO$_2$ without affecting its original crystallinity, thus, enhance the photocatalytic activity, and enrich the H$_2$ production efficiency [212,213]. Different co-catalyst loading methods "techniques" have been successfully applied [38,214,215]; however, the structure and the properties of the co-catalyst were found to play a critical role in achieving superior photocatalytic activity [216]. It has been reported that many structural factors affect the activity of the platinized TiO$_2$, such as the size of Pt NPs [213,217,218], their dispersion of Pt NPs [219,220], the interaction between the metal and the support [221–223], and the chemical state of Pt deposits [220,224]. Nevertheless, all of these factors can be optimized by using proper preparation methods [210,214,220,225,226].

The most commonly adopted techniques for the loading of Pt nanoparticles on the surface of TiO$_2$ include photodeposition [104,105,131,167,210,227], deposition–precipitation [210], chemical reduction [212,228], impregnation [227], electrodeposition [229], and physical mixing [210]. Some of these methods require adding a reducing agent, such as NaBH$_4$, to reduce the metal ions to metal particles. However, the weak adhering of the metal nanoparticles to the semiconductor surface, the larger size of the metal nanoparticles, and the nucleation of isolated metal nanoparticles in the electrolyte are the main problems associated with such methods. Such a poor interaction between the metal nanoparticles and the semiconductor surface negatively affects the electron transfer to the metal, increasing the electron/hole recombination rate [212,230,231]. On the other hand, some techniques need elevated temperatures or an applied bias, and a longer preparation period [128,210,214,232,233].

Photocatalytic hydrogen production over Eosin Y-sensitized Pt-loaded TiO$_2$–ZrO$_2$ mixed oxide photocatalysts was investigated under visible light irradiation by Sreethawong and Yoshikawab [234]. The authors prepared the platinized material by using two different methods, i.e., single-step sol-gel (SSSG) and photochemical deposition (PCD). At the optimum loading ratio (0.5 wt.%) of Pt, the authors found that the platinized photocatalyst prepared by the PCD method exhibited a higher H$_2$ production rate of 2.37 mL/h g comparing to 1.42 mL/h g to that prepared by the SSSG method. They attributed the difference in the photocatalytic activity to the different oxidation states of Pt in both samples. The loaded Pt nanoparticles synthesized by the SSSG method were partly in the oxide form, whereas those prepared via the PCD method consisted of particles in their metallic form having better dispersion on the surface of the semiconductor. Accordingly, the latter provided an efficient charge carrier separation at the interfacial contact between the photochemical-deposited Pt nanoparticles and the TiO$_2$–ZrO$_2$.

Alternatively, the photodeposition method is the most adopted and recommended technique among other loading methods to prepare Pt/TiO$_2$ [128,214]. The interest of the scientific community with the photodeposition method has been greatly expanded since 1978 when Kraeutler and Bernhard employed this technique to synthesize well-dispersed Pt nanoparticles on TiO$_2$ to use this composite in the photocatalytic decomposition of acetic acid to methane [214,235]. Many beneficial features can be controlled during the photodeposition method such as well-defining of co-catalyst nanoparticles, preparing facet-engineered nanoparticles, geometrical distributing of nanoparticles, controlling the size and the oxidation state of the deposited nanoparticles. During the photodeposition process, the metal ions are reduced by the conduction band photogenerated electrons, which leads to a uniform dispersion of the metal nanoparticles on the photocatalyst surface and avoids the self-nucleation of metal particles in the solution [236].

Several structural properties contribute to the photoactivity of the loaded photocatalyst, such as aggregation, Pt-assisted network formation, and Pt dispersion. Wang et al. [222] studied a 1 wt.% platinization of colloidal TiO$_2$ by two methods, i.e., the photodeposition and the mixing with colloidal Pt prepared by chemical reduction of Pt^{4+}. The authors found that during the photocatalytic oxidation of methanol, the quantum yields of HCHO

formation increased by 70% and 50%, for the photocatalyst prepared by photodeposition and mixing, respectively. Additionally, they showed that, in a deoxygenated system, the platinized-TiO_2 prepared by photodeposition method was more efficient for photocatalytic H_2 and HCHO formation than the other platinized sample prepared by physical mixing during the reforming of CH_3OH. The authors explained that Pt clusters on the TiO_2 surface were formed via the photodeposition process, while, Pt particles were surrounded by TiO_2 particles by mixing colloidal Pt with colloidal TiO_2, as shown in Figure 13. Therefore, the better activity of the former is attributed to the better dispersity and the stronger contact between the Pt particles with the TiO_2 surface.
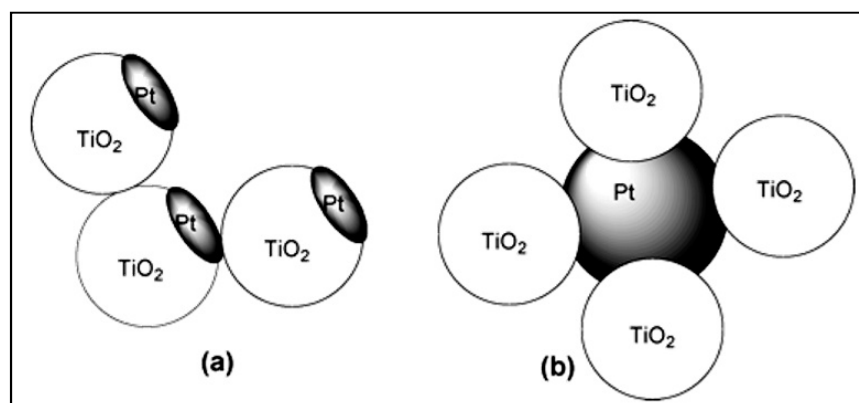

Figure 13. Models of Pt-TiO_2 formed by (**a**) photodeposition of Pt, and (**b**) physical mixing of colloidal Pt and TiO_2. Reprinted with permission from reference [222]. Copyright 2004 American Chemical Society.

Moreover, the deposition of Pt on the surface of TiO_2 enhances the optical property of the Pt-TiO_2. Chen et al. [237] reported that the deposition of Pt on TiO_2 surface via the photodeposition method promoted the optical absorption property of the prepared material to the visible region of light. The authors attributed this enhancement to the formation of Ti^{+3} due to the reduction of the Ti^{+4} during the photodeposition of the Pt. Similarly, F. Li and X. Li [224] found that the deposition of Pt nanoparticles on the TiO_2 surface enhanced the photocatalytic activity due to the formation of a defect energy level near the valence band of TiO_2, as a result of the Ti^{III} formation in the lattice. The authors attributed the formation of Ti^{III} to the interaction between Pt and TiO_2 during the photoreduction process.

Although many reports have shown that the photodeposition technique produces a high active photocatalyst system [210,212], several reports of the metal/semiconductor prepared with other techniques have claimed the contrary [213,225,238]; thus, no general conclusion could be deduced. Apparently, the shape and the nature of Pt NPs besides their interaction with the support are expected to be different by the various platinization methods, which results in diverse photocatalytic behaviors.

5. Photocatalytic Reforming of Aromatic Compounds

Aromatic compounds such as phenols, dyes, and PAHs are important industrial chemicals due to their wide usage. Therefore, the development of novel and simple processes is desired to remove these compounds from the environment, according to the viewpoint of "green chemistry" [239]. Several investigations of photooxidation of such pollutants have been carried out by using TiO_2 and Pt/TiO_2 photocatalysts in the presence of molecular oxygen [113,117,124,240–246].

Due to the low efficiency of overall photocatalytic water splitting, the photoreforming of the organic compounds has shown significantly higher rates and longer-term stability of H_2 production. Therefore, a huge number of photocatalytic reforming studies have been reported. However, simple organic compounds like methanol (the most studied), ethanol, formaldehyde, formic acid, etc., have been mostly used as model pollutants. In this section,

we will focus on the reported investigations that using aromatic compounds like benzene, phenols, dyes, and PAHs as electron donors (hole scavengers), especially over modified TiO_2 materials for the same goal.

As mentioned in Section 4.2, surface-modified TiO_2 and other semiconductors, such as Cu_2O, WO_3, have been widely used as photocatalysts for the photooxidation and the reforming of the hazardous organic pollutants found in wastewater [38,105,130,247]. Upon the total mineralization, the photoreforming process is demonstrated by the following stoichiometric reaction (Equation (8)) [248].

$$C_xH_yO_z + (2x - z)H_2O \rightarrow xCO_2 + (2x - z + y/2)H_2 \tag{8}$$
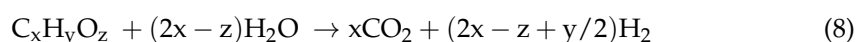
5.1. Monoaromatic and Phenolic-Based Compounds

Benzene is considered a toxic and carcinogenic pollutant. It naturally exists in the environment and is artificially manmade through a wide range of products, such as plastics, paints, mucilage, rubber, and gasoline. It was confirmed that exposure to benzene for a high level or long-time results in several ailments, such as drowsiness, nausea, headache, lightheadedness, dizziness, and cancers. Therefore, it was classified in Category A as a carcinogenic compound by the Environmental Protection Agency.

Hashimoto et al. [247] investigated the photocatalytic H_2 production from different solutions of aliphatic and aromatic compounds using Pt-TiO_2 photocatalyst. Assisted by light energy and in the presence of the photocatalyst, both types of hydrocarbons produced H_2 by reacting with water at room temperature. The maximum H_2 formation was obtained at a 30:1 ratio between the water/benzene mixtures while increasing the benzene ratio decreased the H_2 formation. The authors have claimed that water is the main source of H_2 since no H_2 was detected upon the use of pure benzene in the presence of the Pt-TiO_2 under irradiation. Comparing to the water–alcohol mixture, the authors observed that H_2 and CO_2 are produced at an early stage of irradiation, and the aromatic hydrocarbons produced a higher CO_2 amount than their corresponding derivatives, such as phenol, hydroquinone, and catechol. Therefore, they suggested a higher reactivity of the aromatic hydrocarbons comparing to the hydroxylated aromatic compounds. The authors, hence, proposed that the direct oxidation of benzene by photogenerated holes is the main reaction pathway, followed by the ring-opening producing the corresponding organic acid that decomposes via photo–Kolb reaction (*Path C* in Scheme 2). The authors have excluded phenol and catechol as the main intermediates in this path since benzene swiftly oxidized to muconic acid, whose reactivity is larger than that of benzene itself.

Many other investigations have documented the H_2 formation during the photocatalytic transformation of benzene; however, they have mainly discussed the H_2 formation as a secondary product. These reports focused on other purposes, such as the mechanistic studies of the photocatalytic reaction [12,13,249–251] and the chemical synthesis [162,250,252], rather than the transformation of the aromatic water pollutants into fuels.

On the other hand, phenolic compounds—as we mentioned previously—are one of the most abundant aromatic pollutants in wastewater. Few research groups reported the transformation of these kinds of pollutants into fuels. In 2008, Choi et al. [253] reported the photocatalytic degradation of 4-chlorophenol and bisphenol A on the surface of bare TiO_2 (P25), F-TiO_2, Pt/TiO_2, and F-TiO_2/Pt under anoxic conditions. The authors found that F-TiO_2/Pt exhibited the highest photocatalytic activity towards the conversion of these compounds compared to the other materials. They attributed this activity to the unique synergic effect of two different surface species, i.e., fluoride and platinum, on the photo-induced charge transfer process. Such an effect inhibits the charge recombination on F-TiO_2/Pt as shown in Scheme 3. However, the mineralization of these aromatic compounds could not be achieved for all photocatalysts, since the total organic carbon content in the suspensions remained unaltered during the irradiation. Nevertheless, the authors did not discuss the possibility of molecular hydrogen formation in anoxic conditions and they ignored it in their reaction mechanism.
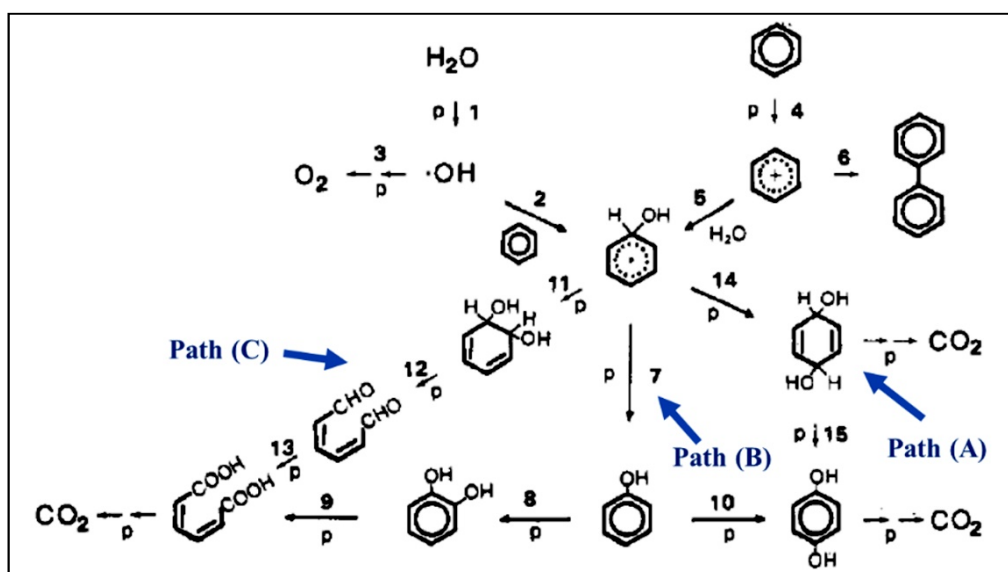
Scheme 2. Reaction scheme of photocatalytic oxidation of benzene in water. Path (A) occurs mainly in the presence of O_2. Path (B) the secondary minor pathway of the reaction, corresponding to the production of the phenol in the system. Path (C): the major pathway of photooxidation of benzene mainly to CO_2. Adapted with permission from reference [247]. Copyright 1984 American Chemical Society.
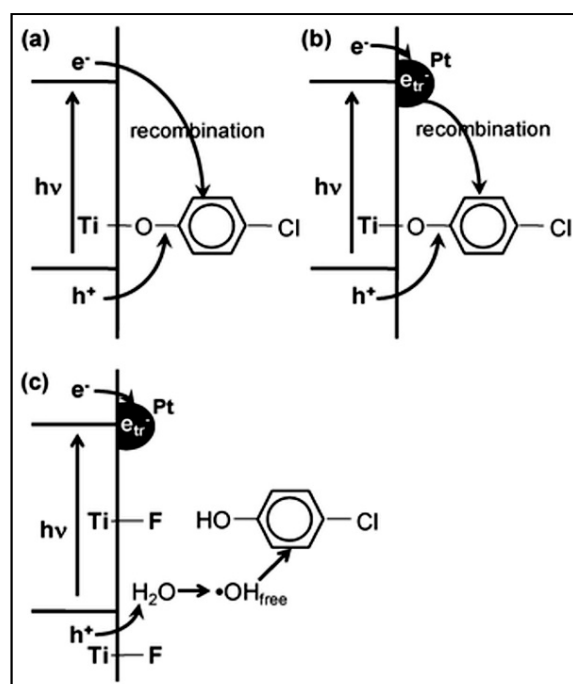
Scheme 3. Photo-induced charge transfer/recombination processes occurring on (**a**) bare TiO_2, (**b**) Pt/TiO_2, and (**c**) $F\text{-}TiO_2/Pt$ in the presence of 4-CP and the absence of O_2. Reprinted with permission from reference [253]. Copyright 2008 Royal Society of Chemistry.

Two years after, the same research group presented similar results, taking into account the simultaneous production of H_2 during the photooxidation of such organic compounds [248]. Interestingly, the authors found that the % photonic efficiencies for H_2 formation during the photooxidation of the simple organic compounds, i.e., dichloroacetic acid and *N*-nitrosodimethylamine were found 0.122 and 0.139, respectively over Pt/TiO_2. These values were higher than those reported for $F\text{-}TiO_2/Pt$, i.e., 0.046 and 0.1, respec-

tively. In contrast, using other aromatic compounds, i.e., hydroquinone, 4-chlorophenol, 4-chlorobenzoic acid, and bisphenol, higher % photonic efficiencies for H_2 were achieved over F-TiO$_2$/Pt (0.094, 0.116, 0.249, 0.334, respectively) than those over Pt/TiO$_2$ (0.052, 0.003, 0.002, 0.044, respectively). The authors reported, additionally, a complete total organic carbons (TOC) removal in the 4-chlorophenol/F-TiO$_2$/Pt suspension after 8-h irradiation.

It is well known that the adsorption of the photodegraded organic intermediates to the photocatalyst surface and the insufficient management of the photo-generated charge carrier inhibits the H_2 evolution reaction and/or the photocatalytic degradation of the organic pollutants in the dual-functional photocatalysis process. [38,104,254]. To this end, Kim et al. [11] studied the enhancement of the dual-functional photocatalysis process by modifying titania photocatalysts with fluoride or phosphate beside the deposition of different metals, i.e., Pt, Pd, Au, Ag, Cu, or Ni. The authors found that the dual-function photocatalysis worked only when both the anion and the metal coexisted on the surface of TiO$_2$, whereas TiO$_2$ modified with a single surface component such as F-TiO$_2$, P-TiO$_2$, or M/TiO$_2$ was inactive under the same experimental condition (Figure 14a). Almost similar dual-functional photocatalysis activities were reported for F-TiO$_2$/Pt and P-TiO$_2$/Pt; however, the synergistic effect greatly depended on the kind of deposited metal and the pH (Figure 14a,b). F-TiO$_2$/Pt was found to be active in the acidic pH region since its activity gradually decreased with increasing pH. In contrast, P-TiO$_2$/Pt exhibited a consistent activity over a wide range of pH, due to the strong chemical bonding of phosphates on TiO$_2$. Therefore, they suggested that P-TiO$_2$/Pt could be more appropriate for practical dual-functional applications (Figure 14c). The authors claimed that the modification of the TiO$_2$ surface with fluorides or phosphates with the deposition of metal acts synergistically to reduce the charge recombination and enhance the interfacial electron transfer, which enhances the photocatalytic activity.
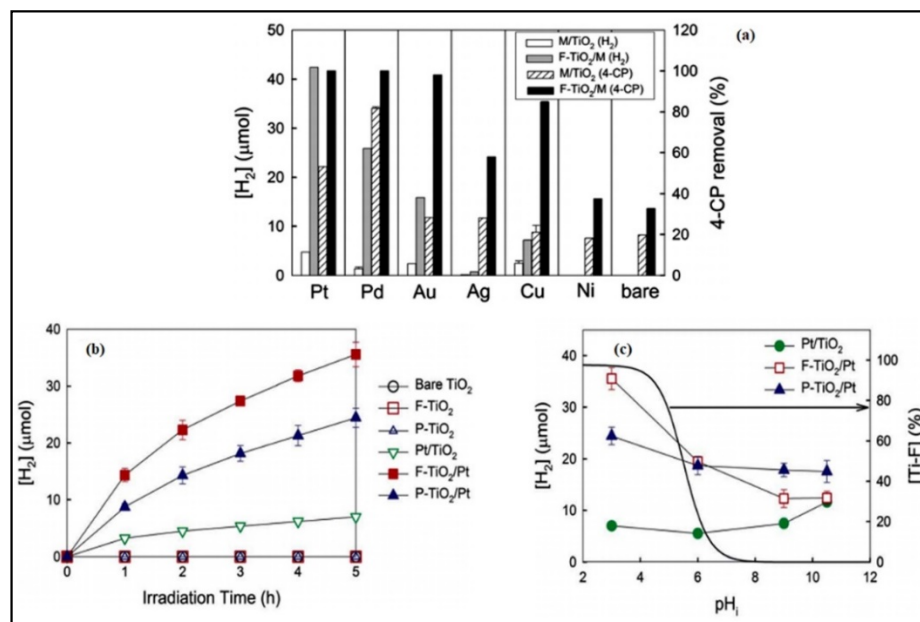
Figure 14. (**a**) Production of H_2 with the simultaneous degradation of 4-CP in the suspension of M/TiO$_2$ and F-TiO$_2$/M (M = Pt, Pd, Au, Ag, Cu, and Ni), (**b**) Production of H_2 in the suspension of bare TiO$_2$, F-TiO$_2$, P-TiO$_2$, Pt/TiO$_2$, F-TiO$_2$/Pt, and P-TiO$_2$/Pt with 4-CP, and (**c**) effect of pH on the production of H_2. Adapted with permission from reference [11]. Copyright 2012 Royal Society of Chemistry.

Furthermore, the enhancement of the dual-functional photocatalytic process toward the simultaneous H_2 formation and 4-chlorophenol degradation was achieved by designing a ternary components photocatalyst [156]. Cr$_2$O$_3$/Rh/SrTiO$_3$ was prepared by covering the

Rh nanoparticles on the surface of SrTiO$_3$ with a thin barrier layer of Cr$_2$O$_3$ to selectively control and maximize the dual-functional photocatalytic activity. Under the same experimental condition, the as-prepared Cr$_2$O$_3$/Rh/SrTiO$_3$ photocatalyst exhibited a higher activity towards H$_2$ production and 4-chlorophenol degradation than that of F-TiO$_2$/Pt and was unaffected by the pH change from the acidic medium to neutral medium (Figure 15).
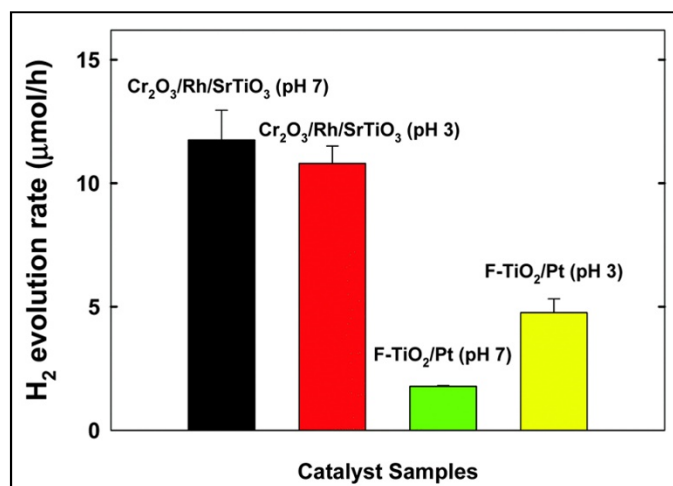
Figure 15. Comparison of the initial photocatalytic H$_2$ production rate between Cr$_2$O$_3$/Rh/SrTiO$_3$ and F-TiO$_2$/Pt photocatalytic systems in the presence of 4-CP. Reprinted from reference [156]. Published by the Royal Society of Chemistry.

According to the authors, the better photocatalytic behavior of Cr$_2$O$_3$/Rh/SrTiO$_3$ can be related to two features. Firstly, the Cr$_2$O$_3$ barrier layer selectively allows the conduction band electrons to be consumed by protons, hindering their transfer to O$_2$ or other electron acceptors. Secondly, the valence band holes are utilized to oxidize both the 4-chlorophenol and H$_2$O (to O$_2$), since the in-situ generated O$_2$ simultaneously and immediately consumed in the oxidation reaction to help in the mineralization of the organic pollutants, as shown in Scheme 4.
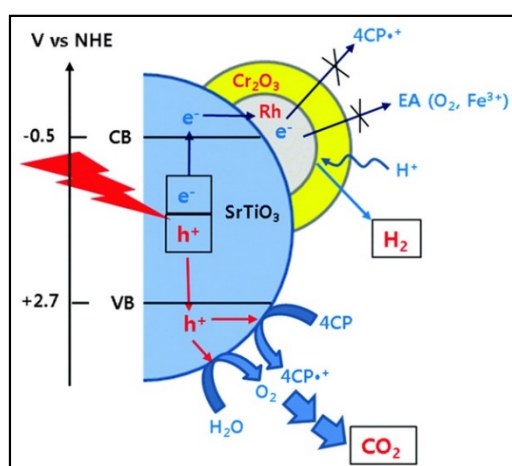
Scheme 4. Schematic illustrations of photocatalytic reaction mechanisms occurring on the surface of Cr$_2$O$_3$/Rh/SrTiO$_3$. Reprinted from reference [156]. Published by the Royal Society of Chemistry.

Cho et al. [255] modified the TiO$_2$ surface by adding the graphene oxide (GO) as a ternary component besides the modification with F and Pt to enhance the dual-functional photocatalytic activity. Pt/GO/TiO$_2$-F showed 1.7 and 3.8 times higher H$_2$ production than Pt/TiO$_2$-F and Pt/GO/TiO$_2$, respectively, during the photocatalytic degradation

of 4-chlorophenol. Since the GO attracts electrons, the interfacial electron transfer was facilitated by the direct contact between GO and the TiO_2 surface, while holes are kept in TiO_2. Such an electron transfer to GO reduces the possibility of recombination of photogenerated charge carriers and extends the lifetime of charge carriers. Moreover, as the work function of Pt is higher than that of GO, i.e., 5.64 and 4.42 eV, respectively, the transfer of photogenerated electrons from GO to Pt is energetically favorable, which enhances the H_2 production. On the other hand, F ions replace the surface hydroxyl groups on the TiO_2 surface, which act as the main hole trap sites. This in turn reduces hole-trapping efficiency and hinders the chemisorption of organic substrates, thus, prevents the direct attack of the organic molecules by the trapped hole. Since the electrons are trapped by Pt, the preferred path of holes is to react with H_2O to generate unbound $OH^\bullet$ radicals that can diffuse out from the surface and react with the organic molecules in the medium. The authors explained that such a ternary hybrid system retards the recombination of the charge carrier and enhances both the H_2 production and 4-chlorophenol degradation, as shown in Scheme 5.
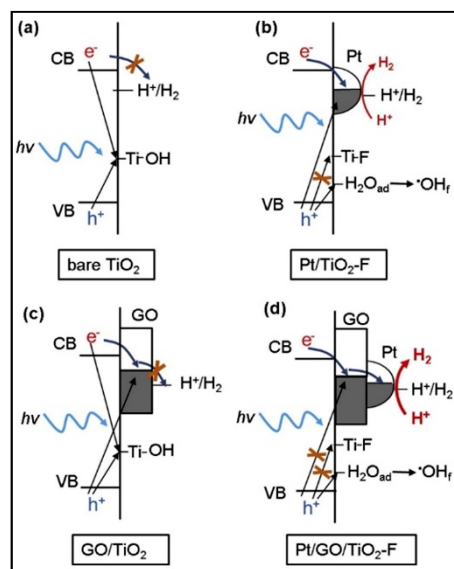
Scheme 5. Schematic illustrations of interfacial charge transfer and recombination occurring on (**a**) bare TiO_2, (**b**) Pt/TiO_2–F, (**c**) GO/TiO_2, and (**d**) Pt/GO/TiO_2–F in the absence of O_2. Reprinted with permission from reference [255]. Copyright 2015 Elsevier B.V.

Recently, many efforts have been made to use visible-light active dual-functional photocatalysts. For example, the two-dimensional (2D) black phosphorous/2D carbon nitride (2D BP/2D C_3N_4) was synthesized and employed for efficient H_2 evolution with the simultaneous photodegradation of bisphenol A pollutant (BPA) [256]. The H_2 evolution rate and the BPA removal over 2D C_3N_4 nanosheets were found to be ~45 $\mu mol \cdot h^{-1} \cdot g^{-1}$ and 43%, respectively. Upon the introduction of 2D BP, both the H_2 production rate and the simultaneous BPA removal were improved. The optimum ratio of 5% 2D BP exhibits an H_2 evolution rate of 259.04 $\mu mol \cdot h^{-1} \cdot g^{-1}$ and BPA removal rate of 88% with an external quantum efficiency of 0.56% at 420 nm (Figure 16a). The authors attributed the high efficiency of this material to the intimate electronic interaction between 2D BP and 2D C_3N_4, besides the excellent charge mobility between the two composites.
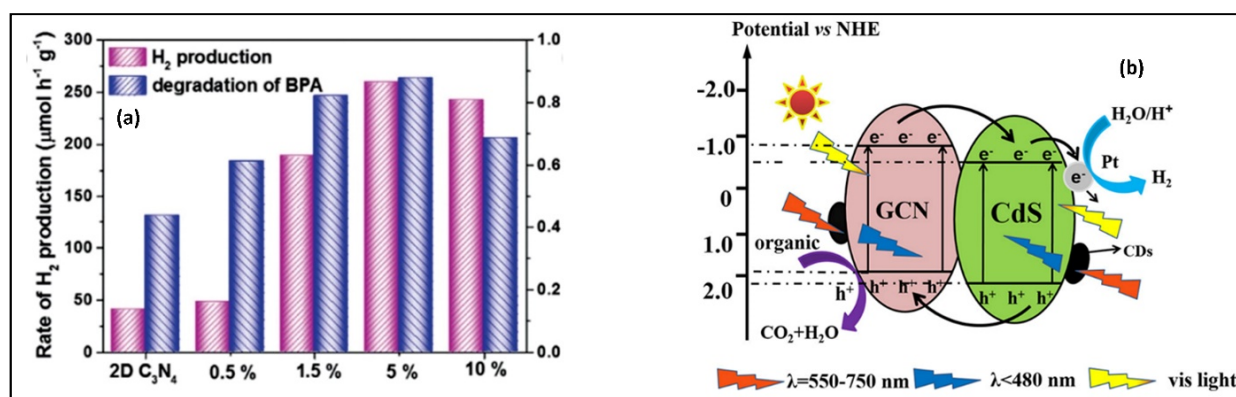
Figure 16. (**a**) Production of H_2 with simultaneous degradation in the presence of bisphenol A pollutant (BPA) over 2D C_3N_4 coupled with different amounts of 2D BP. Reprinted with permission from reference [256]. Copyright 2019 Elsevier B.V. (**b**) Illustration for the Photocatalytic Mechanism over the 3%CDs/10%CdS/GCN Catalyst under visible-light irradiation. Reprinted with permission from reference [257]. Copyright 2018 Royal Society of Chemistry.

Another effort was exerted towards the development of new materials possessing optical properties in the visible light region. Jiang et al. [257] prepared a photocatalyst consists of carbon quantum dots/CdS quantum dots/g-C_3N_4 (CDs/CdS/GCN) photocatalyst composite. The photocatalytic activity of this material under visible-light illumination was evaluated for concurrent H_2 production and the decomposition of typical wastewater pollutants like p-chlorophenol, bisphenol A, and tetracycline. The 3%CDs/10%CdS/GCN photocatalyst exhibited the best photocatalytic efficiency under the visible-light irradiation for H_2 evolution from water splitting in an aqueous solution containing organic pollutants (Figure 16b). The addition of p-chlorophenol decreased the photocatalytic H_2 evolution rate compared with the pure water system, due to the consumption of some photogenerated electrons in the degradation of p-chlorophenol. Although the photocatalytic degradation rate of p-chlorophenol was higher than those of bisphenol A and tetracycline, the H_2 evolution rate increased with the addition of bisphenol A or tetracycline. The authors have explained such a result by the consumption of all photogenerated electrons to split water for H_2 production.

On the other hand, some reports have shown the inability to use phenol as a sacrificial reagent in the dual functional photocatalytic processes. Mogyorósi et al. [258] investigated the photocatalytic H_2 production and the decomposition of various organics using 1% Pt-, Au-, and Ag-deposited on the surface of Degussa P25 photocatalysts. The photocatalytic decomposition of oxalic acid and formic acid was increased upon the deposition of noble metals compared to that of the bare photocatalyst. However, in phenol containing system, the authors reported a decrease in the decomposition activity, indicating that the noble metals block the active sites on the surface of the photocatalyst. On the other hand, they practically reported no H_2 production over the bare and the modified P25 in the presence of phenol as a sacrificial reagent. While a very high quantum yield for H_2 production over Pt-TiO_2 photocatalyst was reported in the presence of oxalic and formic acids. They have concluded that O_2 was a requirement for the photooxidation of phenol in presence of any photocatalysts since no decomposition was detected in its absence. Hence, the inhibition of phenol photooxidation in anoxic conditions negatively affects the ability of H_2 production.

5.2. Dyes and Polyaromatic-Based Pollutants

A wide variety of photocatalysts was designed to achieve the goal of the dual-functional photocatalysis technology; simultaneous H_2 production and wastewater purification by the degradation of the persistent dyes [38,39,189,259–262]. The production of hydrogen with a simultaneous degradation of azo dye solution (commercial name Acid Orange 7; AO7) using the well-known photocatalyst Pt/TiO_2 suspensions was examined by Patsoura [261] under UV-vis light. The authors have investigated the effect of the dye

concentration, the pH, and the temperature on the H_2 production rate. Besides, the effect of the Pt loading ratio on the H_2 formation rate was thermodynamically investigated through the dynamic of the charge carrier during the reaction. In the absence of the Azo-dye and after the deposition of Pt (0.5 wt.%) on the TiO_2 surface, the H_2 production rate increased to a maximum during the irradiation before dropping to a very low steady-state rate value comparable to those obtained over bare TiO_2. Although, it is well known that bare TiO_2 is inactive for the H_2 production due to the driving force for this reaction is small, and the presence of a large overpotential for the H_2 evolution [263], the authors attributed such activity to the presence of (i) metal or organic impurities in the semiconductor; (ii) partially reduced titania species; (iii) small size semiconductor particles that exhibit a higher efficiency in photocatalytic reactions. The authors also reported an improvement in the H_2 formation during the photo-induced water splitting reaction over Pt/TiO_2 by increasing the pH and the temperature. Interestingly, the presence of a small quantity of Azo dye in the reaction medium significantly enhanced the H_2 formation rate, which depends on dye concentration, solution pH, and to a lesser extent to the solution temperature. They found that using a higher dye concentration resulted in increasing H_2 formation over a longer reaction period. However, afterward, the formation rate was decreased to a steady-state value comparable to that obtained in the absence of the azo dye. The authors have attributed this decrease to the complete mineralization of the AO7 by-products in the reaction solution, due to their oxidation by consuming the photogenerated oxygen from the surface of the photocatalyst.

In the same study, another two azo dyes, namely Basic Blue 41 and Basic Red 46 have been tested at a neutral pH solution to ascertain that the use of a dye is generally beneficial for the rate of H_2 production. Similar behavior to the addition of AO7 was observed for the other azo dyes. The H_2 formation rate increased during the first few hours of irradiation and then progressively dropped to steady-state values similar to those obtained for pure water.

The authors have also highlighted that the adsorption of the reaction intermediates on Pt cannot be effectively removed under the experiment conditions, which leads to retarding the H_2 evolution. This behavior had been observed in many similar photocatalytic systems dealing with the TiO_2 and aromatic compounds [104,167,247,250].

On the other hand, increasing pH from 4 to 10 resulted in a significant increase in the maximum formation rate from 0.28 to 0.67 µmol/min, which was related to the enhanced kinetics of dye degradation with increasing the solution pH. According to these authors, this enhancement indicating that the rate of H_2 production is limited by the rate of consumption of photogenerated O_2. Therefore, they conclude that the azo dye acts as a sacrificial agent that rapidly remove the photogenerated holes and consume the photogenerated oxygen. This suppresses electron-hole and O_2-H_2 recombination, enhancing the H_2 production until complete degradation of the dye to CO_2 and inorganic ions.

The modification of the TiO_2 in a way that increases the adsorption of the organic molecules on its surface is considered one of the methods that enhance the photocatalytic activity since the direct hole transfer to the organic molecules is dominant [264,265]. Bifunctional TiO_2 photocatalysts have been developed by Kim et al. [266] through the modification of the surface of TiO_2 with two different components, platinum, and Nafion ($Pt/TiO_2/Nf$). The simultaneous H_2 production and rhodamine B (RhB) degradation was successfully achieved using $Pt/TiO_2/Nf$ under visible light ($\lambda > 420$ nm). $Pt/TiO_2/Nf$ exhibited high activity for H_2 production in the presence of RhB as a photosensitizer and organic dye pollutant, besides EDTA as an electron donor. However, the modification with only one component, i.e., Pt or Nf, resulted in a negligible activity for H_2 production under the same experimental conditions. According to the authors, the negative charge of the Nafion layer improves the adsorption of cationic RhB and pulls protons to the surface of TiO_2 through electrostatic attraction, enhancing the RhB photooxidation. Simultaneously, these protons are reduced to H_2 on the deposited Pt that acts as an electron sink and a temporary electron reservoir for the reduction half-reaction. The authors found that RhB

was not degraded in the absence of EDTA, which is involved in the reaction mechanism by converting the RhB to *N*-deethylation. In this dual-functional photocatalytic system, a 20 μM (0.6 μmol) of RhB approximately produced 70 μmol of H_2, while the RhB and its intermediates were completely removed over 12 h period.

Polycyclic aromatic hydrocarbons (PAHs) are a kind of semi-volatile persistent aromatic pollutants [267]. These compounds are frequently detected in different types of wastewater [58,267]. As for many other pollutants, advanced oxidative processes based on photocatalysis have often been reported for the removal of PAHs [268,269]. Although several studies have explored their photocatalytic degradation in anoxic conditions [268,270,271]; however, very limited reports on the remediation of PAHs with simultaneous H_2 production had been documented in the literature [104,167]. On the other hand, several reports on the simplest aromatic compound benzene have proved its ability to act as a sacrificial electron donor (hole scavenger) to photo-catalyze molecular hydrogen [247,250,251]. Bahnemann's research group has considered this shortage in the literature and spotted the light on employing these compounds as sacrificial electron donors in the dual-functional photocatalysis system [104,167,272].

The hydrogen production with the simultaneous degradation of the simplest PAH compounds naphthalene based on Pt/TiO_2 has been investigated by the Bahnemann research group [167]. In this study, two different commercial TiO_2 photocatalysts, Aeroxide P25 ($ATiO_2$) and Sachtleben Hombikat UV100 ($HTiO_2$) were loaded with different fractional ratios of Pt nanoparticles using the photodeposition method. The aim was to evaluate the role of the loaded Pt on hydrogen production and the simultaneous degradation of naphthalene. The 0.5 wt.% Pt was found to be the optimum loading ratio on the surface of $HTiO_2$, which increased the conversion of naphthalene from 71% for bare $HTiO_2$ to 82% and produces 6 μmol of H_2 (Figure 17). However, the authors found that using a higher Pt content than the optimal platinization ratio inhibited both processes, the H_2 formation, and naphthalene photooxidation. On the other hand, they claimed that loading $ATiO_2$ with the Pt nanoparticles regardless of the platinization ratio decreased naphthalene conversion, while no dependency between the Pt ratio and the H_2 formation rate was found since all OF the platinized $ATiO_2$ materials showed a similar H_2 formation of around 3 μmol.
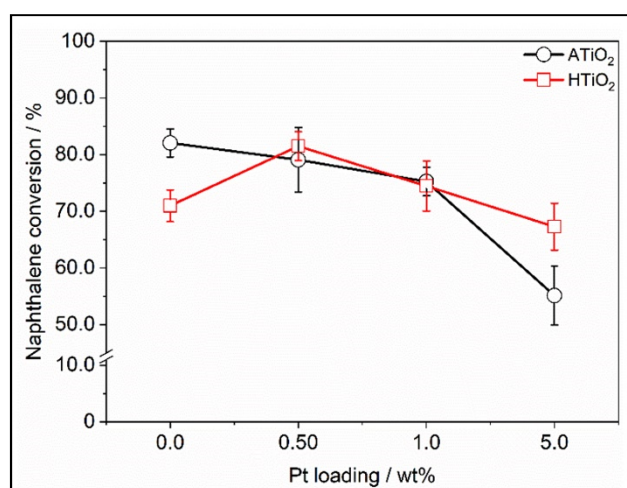
Figure 17. Naphthalene conversion in the presence of TiO_2-based photocatalysts loaded with different % of Pt nanoparticles. Reprinted with permission from reference [167].

Based on the EPR technique, the authors concluded that the Pt NPs on $ATiO_2$ acted as recombination centers for the photogenerated charge carrier. They have additionally related the decreases of H_2 formation rate and naphthalene conversion during the photocatalytic process to the deactivation of the photocatalyst due to adsorption of the formed intermediates on the surface of the photocatalyst. Interestingly, the authors demonstrated

that the reforming of PAHs over the Pt-HTiO$_2$ exhibits higher photonic efficiencies than that of their corresponding hydroxylated compounds, such as 1 and 2-naphthols.

In another study, the effect of the co-catalyst loading methods on the physicochemical properties of the dual-functional photocatalyst was studied by the same research group [272]. Anatase TiO$_2$ (Sachtleben Hombikat UV100) was loaded with Pt nanoparticles using two alternative methods: photodeposition by reduction of PtCl$_6^{2-}$ (Pt$_{PD}$-TiO$_2$) and physical mixing of TiO$_2$ with Pt nanoparticles synthesized by laser ablation (Pt$_{LA}$-TiO$_2$). Both as-prepared materials were fully characterized, and their photocatalytic activities were evaluated for the photoreforming of naphthalene and methanol. Over both photocatalysts, the authors reported a huge difference in H$_2$ formation between the two-electron donors, which can be related to the different nature of the organic compounds. Methanol reacts swiftly with the photogenerated holes, while the reaction of naphthalene involved multi-complicated steps. On the other hand, Pt$_{PD}$-TiO$_2$ exhibited better photocatalytic activity toward naphthalene oxidation and H$_2$ formation compared to Pt$_{LA}$-TiO$_2$. Based on the transient absorption spectroscopy and the electron paramagnetic spectroscopy techniques, the higher activity of Pt$_{PD}$-TiO$_2$ was related to the better charge carrier transfer between the TiO$_2$ and the loaded Pt nanoparticles. The authors explained these results by the better dispersion of Pt nanoparticles and their strong interaction with the surface of TiO$_2$.

The mechanism of the dual-functional photocatalysis process for molecular hydrogen formation concurrent with naphthalene degradation over Pt-TiO$_2$ (Hombikat UV100) has been investigated [104]. The authors reported photonic efficiencies of 0.33% and 0.970% for naphthalene conversion and H$_2$ formation, respectively, under simulated sunlight. After 4 h irradiation, the authors were able to determine the formed organic by-products in the system by the mean of gas chromatography - mass spectrometry, high-performance liquid chromatography, and high pressure ion chromatography techniques. Moreover, through the spin-trapping experiments, they proved that only the photogenerated holes play the main role in the photooxidation of naphthalene, while, the isotopic labeling analyses showed that the evolved H$_2$ originated mainly from water. According to these results, the authors suggested the following mechanism for hydroxylation of naphthalene (Equations (9)–(15)), while the total mineralization mechanism was shown in Scheme 6.

$$TiO_2 \rightarrow n(e^- + h^+)TiO_2 \tag{9}$$

(where $-\cdot OH_s$: surface trapped holes and OH_s^- : surface hydroxyl ion)

$$\tag{10}$$

$$\tag{11}$$

$$\tag{12}$$

$$\tag{13}$$

$$Pt - TiO_2[e^-] + H_{(ads)}^+ \rightarrow Pt - TiO_2 + H_{(ads)}^\bullet \tag{14}$$

$$2H_{(ads)}^\bullet \rightarrow H_2(\uparrow) \tag{15}$$
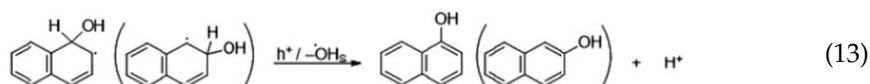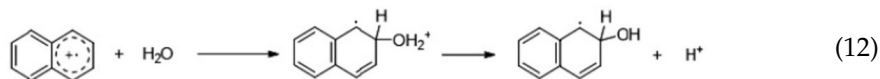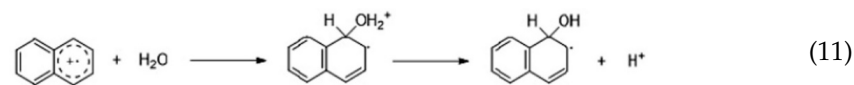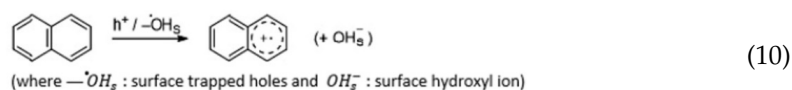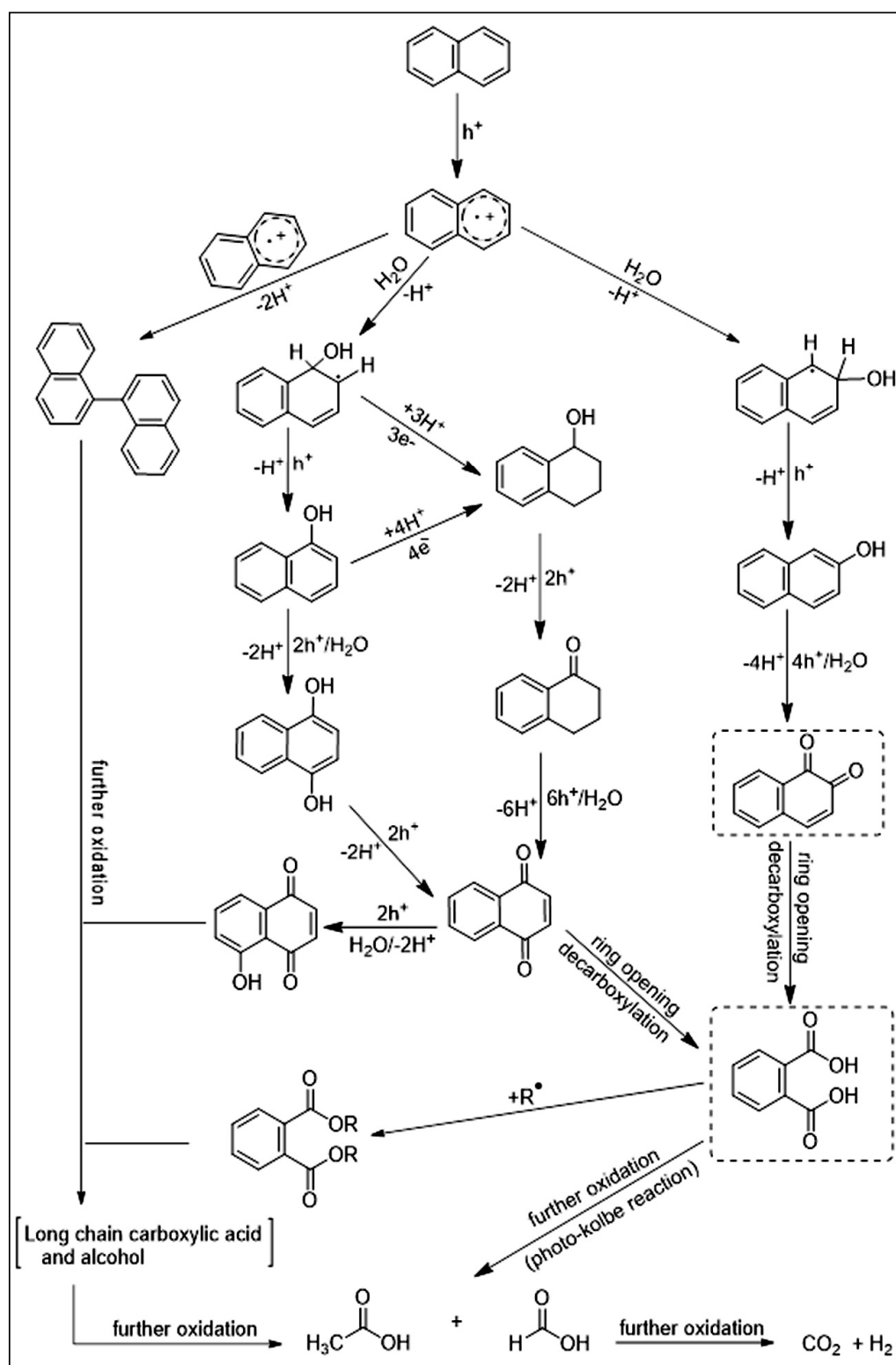
Scheme 6. Proposed mechanism for the photocatalytic reforming of naphthalene over Pt-UV100 under simulated sunlight. Note: compounds inside the dashed square were not detected during the by-products identification. Reprinted with permission from reference [104]. Copyright 2020 Royal Society of Chemistry.

6. Conclusions

The increase in the quantity and quality of pollutants associated with industrial progress and population growth makes it necessary to match this increase with efficient and sustainable ways to treat it; hence, the urge to develop new materials or to modify and/or enhance the performance of some existing materials. There is no doubt that abundance and low cost are advantages that every semiconductor must meet for their application in large-scale photocatalytic systems. These two properties turned TiO_2 into an attractive material in this field—attractive enough to devote large scientific efforts to overcome its main limitations: fast charge carrier recombination rates and a relatively large bandgap (3.2 eV), so that only UV radiation can activate it. However, the adopted strategies to improve TiO_2 performance and make it more appealing for large-scale applications— some of these strategies are discussed in this review, and are, to a large extent working, and seem promising. However, miniaturizing or synthesizing in the nanoscale is not the only way to achieve high efficiency. The fast recombination of the photogenerated charges could be significantly reduced by the loading of co-catalyst, which is normally noble metal nanoparticles. The high cost of the noble metals and their limited availability make them a not idealistic choice. One more time, cost-effectiveness comes into play but this time as a limiting factor. The search for co-catalysts that demonstrate high efficiency combined with cost efficiency is a challenging issue in photocatalysis. The wide scale of chemical and physical properties of both pollutants and semiconductors could anticipate the use of oxide-oxide or metal-oxide hetero nanostructures to create new properties that achieve higher performance and enhanced ability to remove, reform, or degrade pollutants. Not to mention that heterostructures could demonstrate the same function as a catalyst and co-catalyst without the resolve to high-cost noble metals, which could be a working strategy with enormous numbers of materials. Finally, despite a large amount of photocatalytic reforming studies, there is a huge deficiency in the investigation of the photocatalytic reforming of aromatic-based pollutants, especially the PAHs. Such pollutants have shown the ability for photocatalytic oxidation in the oxygen atmosphere; however, few reports have been published that deal with the H_2 production based on their photoreforming. Hence, this research line can be a rich area for further future investigation.

References

1. Liew, W.T.; Adhitya, A.; Srinivasan, R. Sustainability trends in the process industries: A text mining-based analysis. *Comput. Ind.* **2014**, *65*, 393–400. [CrossRef]
2. Mechhoud, E.; Rouainia, M.; Rodriguez, M. A new tool for risk analysis and assessment in petrochemical plants. *Alex. Eng. J.* **2016**, *55*, 2919–2931. [CrossRef]
3. Rovira, E.; Cuadras, A.; Aguilar, X.; Esteban, L.; Borràs-Santos, A.; Zock, J.-P.; Sunyer, J. Asthma, respiratory symptoms and lung function in children living near a petrochemical site. *Environ. Res.* **2014**, *133*, 156–163. [CrossRef]
4. Villanueva, F.; Tapia, A.; Lara, S.; Amo-Salas, M. Indoor and outdoor air concentrations of volatile organic compounds and NO_2 in schools of urban, industrial and rural areas in Central-Southern Spain. *Sci. Total Environ.* **2018**, *622–623*, 222–235. [CrossRef]

5. Bari, M.A.; Kindzierski, W.B. Ambient volatile organic compounds (VOCs) in communities of the Athabasca oil sands region: Sources and screening health risk assessment. *Environ. Pollut.* **2018**, *235*, 602–614. [CrossRef]

6. Matthews, R.W. Purification of water with near—u.v. illuminated suspensions of titanium dioxide. *Water Res.* **1990**, *24*, 653–660. [CrossRef]

7. Matthews, R.W. An adsorption water purifier with in situ photocatalytic regeneration. *J. Catal.* **1988**, *113*, 549–555. [CrossRef]

8. Grigoryan, H.; Edmands, W.M.B.; Lan, Q.; Carlsson, H.; Vermeulen, R.; Zhang, L.; Yin, S.N.; Li, G.L.; Smith, M.T.; Rothman, N.; et al. Adductomic signatures of benzene exposure provide insights into cancer induction. *Carcinogenesis* **2018**, *39*, 661–668. [CrossRef]

9. He, C.; Cheng, J.; Zhang, X.; Douthwaite, M.; Pattisson, S.; Hao, Z. Recent advances in the catalytic oxidation of volatile organic compounds: A review based on pollutant sorts and sources. *Chem. Rev.* **2019**, *119*, 4471–4568. [CrossRef]

10. Alegría, M.; Aliaga, J.; Ballesteros, L.; Sotomayor-Torres, C.; González, G.; Benavente, E. Layered nanocomposite 2D-TiO$_2$ with Cu$_2$O nanoparticles as an efficient photocatalyst for 4-Chlorophenol degradation and hydrogen evolution. *Top. Catal.* **2020**. [CrossRef]

11. Kim, J.; Monllor-Satoca, D.; Choi, W. Simultaneous production of hydrogen with the degradation of organic pollutants using TiO$_2$ photocatalyst modified with dual surface components. *Energy Environ. Sci.* **2012**, *5*, 7647–7656. [CrossRef]

12. Montoya, J.F.; Bahnemann, D.W.; Peral, J.; Salvador, P. Catalytic role of TiO$_2$ terminal oxygen atoms in liquid-phase photocatalytic reactions: Oxidation of aromatic compounds in anhydrous acetonitrile. *ChemPhysChem* **2014**, *15*, 2311–2320. [CrossRef] [PubMed]

13. Montoya, J.F.; Ivanova, I.; Dillert, R.; Bahnemann, D.W.; Salvador, P.; Peral, J. Catalytic role of surface oxygens in TiO$_2$ photooxidation reactions: Aqueous benzene photooxidation with Ti^{18}O$_2$ under anaerobic conditions. *J. Phys. Chem. Lett.* **2013**, *4*, 1415–1422. [CrossRef]

14. Teras, L.R.; Diver, W.R.; Deubler, E.L.; Krewski, D.; Flowers, C.R.; Switchenko, J.M.; Gapstur, S.M. Residential ambient benzene exposure in the United States and subsequent risk of hematologic malignancies. *Int. J. Cancer* **2019**, *145*, 2647–2660. [CrossRef]

15. Mustieles, V.; Fernández, M.F.; Martin-Olmedo, P.; González-Alzaga, B.; Fontalba-Navas, A.; Hauser, R.; Olea, N.; Arrebola, J.P. Human adipose tissue levels of persistent organic pollutants and metabolic syndrome components: Combining a cross-sectional with a 10-year longitudinal study using a multi-pollutant approach. *Environ. Int.* **2017**, *104*, 48–57. [CrossRef] [PubMed]

16. Zhang, X.; Gao, B.; Creamer, A.E.; Cao, C.; Li, Y. Adsorption of VOCs onto engineered carbon materials: A review. *J. Hazard. Mater.* **2017**, *338*, 102–123. [CrossRef]

17. Liu, L.; Li, J.; Zhang, H.; Li, L.; Zhou, P.; Meng, X.; Guo, M.; Jia, J.; Sun, T. In situ fabrication of highly active γ-MnO$_2$/SmMnO$_3$ catalyst for deep catalytic oxidation of gaseous benzene, ethylbenzene, toluene, and o-xylene. *J. Hazard. Mater.* **2019**, *362*, 178–186. [CrossRef]

18. Mosmeri, H.; Gholami, F.; Shavandi, M.; Dastgheib, S.M.M.; Alaie, E. Bioremediation of benzene-contaminated groundwater by calcium peroxide (CaO$_2$) nanoparticles: Continuous-flow and biodiversity studies. *J. Hazard. Mater.* **2019**, *371*, 183–190. [CrossRef]

19. Markham, S.C. Photocatalytic properties of oxides. *J. Chem. Educ.* **1955**, *32*, 540. [CrossRef]

20. Fujishima, A.; Honda, K. Electrochemical photolysis of water at a semiconductor electrode. *Nature* **1972**, *238*, 37–38. [CrossRef]

21. Sabarinathan, M.; Harish, S.; Archana, J.; Navaneethan, M.; Ikeda, H.; Hayakawa, Y. Highly efficient visible-light photocatalytic activity of MoS$_2$–TiO$_2$ mixtures hybrid photocatalyst and functional properties. *RSC Adv.* **2017**, *7*, 24754–24763. [CrossRef]

22. Liu, X.; Zhai, H.; Wang, P.; Zhang, Q.; Wang, Z.; Liu, Y.; Dai, Y.; Huang, B.; Qin, X.; Zhang, X. Synthesis of a WO$_3$ photocatalyst with high photocatalytic activity and stability using synergetic internal Fe^{3+} doping and superficial Pt loading for ethylene degradation under visible-light irradiation. *Catal. Sci. Technol.* **2019**, *9*, 652–658. [CrossRef]

23. Ramadan, W.; Shaikh, P.A.; Ebrahim, S.; Ramadan, A.; Hannoyer, B.; Jouen, S.; Sauvage, X.; Ogale, S. Highly efficient photocatalysis by BiFeO$_3$/α(γ)-Fe$_2$O$_3$ ferromagnetic nano p/n junctions formed by dopant-induced phase separation. *J. Nanopart. Res.* **2013**, *15*, 1848. [CrossRef]

24. Mishra, M.; Chun, D.-M. α-Fe$_2$O$_3$ as a photocatalytic material: A review. *Appl. Catal. A* **2015**, *498*, 126–141. [CrossRef]

25. Ebrahim, S.; Ramadan, W.; Ali, M. Structural, optical and ferromagnetic properties of cobalt doped CdTe quantum dots. *J. Mater. Sci. Mater. Electron.* **2016**, *27*, 3826–3833. [CrossRef]

26. Kaur, R.; Rana, A.; Singh, R.K.; Chhabra, V.A.; Kim, K.-H.; Deep, A. Efficient photocatalytic and photovoltaic applications with nanocomposites between CdTe QDs and an NTU-9 MOF. *RSC Adv.* **2017**, *7*, 29015–29024. [CrossRef]

27. Huang, C.-W.; Nguyen, B.-S.; Wu, J.C.S.; Nguyen, V.-H. A current perspective for photocatalysis towards the hydrogen production from biomass-derived organic substances and water. *Int. J. Hydrog. Energy* **2020**, *45*, 18144–18159. [CrossRef]

28. Serpone, N. Is the band gap of pristine TiO$_2$ narrowed by anion- and cation-doping of titanium dioxide in second-generation photocatalysts? *J. Phys. Chem. B* **2006**, *110*, 24287–24293. [CrossRef]

29. Fouda, A.; Hassan, S.E.-D.; Saied, E.; Azab, M.S. An eco-friendly approach to textile and tannery wastewater treatment using maghemite nanoparticles (γ-Fe$_2$O$_3$-NPs) fabricated by Penicillium expansum strain (K-w). *J. Environ. Chem. Eng.* **2021**, *9*, 104693. [CrossRef]

30. Angaru, G.K.R.; Choi, Y.L.; Lingamdinne, L.P.; Choi, J.S.; Kim, D.S.; Koduru, J.R.; Yang, J.K.; Chang, Y.Y. Facile synthesis of economical feasible fly ash-based zeolite-supported nano zerovalent iron and nickel bimetallic composite for the potential removal of heavy metals from industrial effluents. *Chemosphere* **2021**, *267*, 128889. [CrossRef]

31. Al-Madanat, O.; Jiries, A.; Batarseh, M.; Al-Nasir, F. Indoor and outdoor pollution with heavy metals in Al-Karak city, Jordan. *J. Int. Environ. Appl. Sci.* **2017**, *12*, 131–139.

32. Al-Nasir, F.M.; Jiries, A.G.; Al-Rabadi, G.J.; Alu'datt, M.H.; Tranchant, C.C.; Al-Dalain, S.A.; Alrabadi, N.; Madanat, O.Y.; Al-Dmour, R.S. Determination of pesticide residues in selected citrus fruits and vegetables cultivated in the Jordan Valley. *LWT* **2020**, *123*, 109005. [CrossRef]

33. Lei, M.; Gao, Q.; Zhou, K.; Gogoi, P.; Liu, J.; Wang, J.; Song, H.; Wang, S.; Liu, X. Catalytic degradation and mineralization mechanism of 4-chlorophenol oxidized by phosphomolybdic acid/H_2O_2. *Sep. Purif. Technol.* **2021**, *257*, 117933. [CrossRef]

34. Kuttiani Ali, J.; Maher Chabib, C.; Abi Jaoude, M.; Alhseinat, E.; Teotia, S.; Patole, S.; Hussain Anjum, D.; Qattan, I. Enhanced removal of aqueous phenol with polyimide ultrafiltration membranes embedded with deep eutectic solvent-coated nanosilica. *Chem. Eng. J.* **2021**, *408*, 128017. [CrossRef]

35. Al Nasir, F.; Batarseh, M.I. Agricultural reuse of r 456545eclaimed water and uptake of organic compounds: Pilot study at Mutah University wastewater treatment plant, Jordan. *Chemosphere* **2008**, *72*, 1203–1214. [CrossRef]

36. Torres-Pinto, A.; Sampaio, M.J.; Silva, C.G.; Faria, J.L.; Silva, A.M.T. Metal-free carbon nitride photocatalysis with in situ hydrogen peroxide generation for the degradation of aromatic compounds. *Appl. Catal. B* **2019**, *252*, 128–137. [CrossRef]

37. Alrabadi, G.; Al-Nasir, F.; Jiries, A.; Al-Dmour, R.; Madanat, O.; Al-Dalain, S. Polychlorinated biphenyls residue in citrus and vegetables in the Jordan Valley, Jordan. *JJEES* **2019**, *10*, 247–251.

38. Lin, Z.; Li, L.; Yu, L.; Li, W.; Yang, G. Dual-functional photocatalysis for hydrogen evolution from industrial wastewaters. *Phys. Chem. Chem. Phys.* **2017**, *19*, 8356–8362. [CrossRef]

39. Puga, A.V.; Barka, N.; Imizcoz, M. Simultaneous H_2 production and bleaching via solar photoreforming of model dye-polluted wastewaters on metal/titania. *ChemCatChem* **2020**. [CrossRef]

40. AlSalka, Y.; Karabet, F.; Hashem, S. Development and optimisation of quantitative analytical method to determine BTEX in environmental water samples using HPLC-DAD. *Anal. Methods* **2010**, *2*, 1026–1035. [CrossRef]

41. Villegas, L.G.C.; Mashhadi, N.; Chen, M.; Mukherjee, D.; Taylor, K.E.; Biswas, N. A short review of techniques for phenol removal from wastewater. *Curr. Pollut. Rep.* **2016**, *2*, 157–167. [CrossRef]

42. Michałowicz, J.; Duda, W. Phenols—Sources and toxicity. *Pol. J. Environ. Stud.* **2007**, *16*, 347–362.

43. Zango, Z.U.; Sambudi, N.S.; Jumbri, K.; Ramli, A.; Abu Bakar, N.H.H.; Saad, B.; Rozaini, M.N.H.; Isiyaka, H.A.; Osman, A.M.; Sulieman, A. An overview and evaluation of highly porous adsorbent materials for polycyclic aromatic hydrocarbons and phenols removal from wastewater. *Water* **2020**, *12*, 2921. [CrossRef]

44. Anku, W.W.; Mamo, M.A.; Govender, P.P. *Phenolic Compounds in Water: Sources, Reactivity, Toxicity and Treatment Methods, Phenolic Compounds—Natural Sources, Importance and Applications*; IntechOpen-Open Science Open Minds: London, UK, 2017. [CrossRef]

45. Igbinosa, E.O.; Odjadjare, E.E.; Chigor, V.N.; Igbinosa, I.H.; Emoghene, A.O.; Ekhaise, F.O.; Igiehon, N.O.; Idemudia, O.G. Toxicological profile of chlorophenols and their derivatives in the environment: The public health perspective. *Sci. World J.* **2013**, *2013*, 460215. [CrossRef] [PubMed]

46. Tang, W.Z.; Huang, C.P. Effect of chlorine content of chlorinated phenols on their oxidation kinetics by Fenton's reagent. *Chemosphere* **1996**, *33*, 1621–1635. [CrossRef]

47. Alsalka, Y.; Karabet, F.; Hashem, S. Evaluation of electrochemical processes for the removal of several target aromatic hydrocarbons from petroleum contaminated water. *J. Environ. Monit.* **2011**, *13*, 605–613. [CrossRef]

48. Drwal, E.; Rak, A.; Gregoraszczuk, E.L. Review: Polycyclic aromatic hydrocarbons (PAHs)-Action on placental function and health risks in future life of newborns. *Toxicology* **2019**, *411*, 133–142. [CrossRef]

49. Patel, A.B.; Shaikh, S.; Jain, K.R.; Desai, C.; Madamwar, D. Polycyclic aromatic hydrocarbons: Sources, toxicity, and remediation approaches. *Front. Microbiol.* **2020**, *11*, 562813. [CrossRef] [PubMed]

50. Abdel-Shafy, H.I.; Mansour, M.S.M. A review on polycyclic aromatic hydrocarbons: Source, environmental impact, effect on human health and remediation. *Egypt. J. Pet.* **2016**, *25*, 107–123. [CrossRef]

51. Mastral, A.M.; Callén, M.S. A review on polycyclic aromatic hydrocarbon (PAH) emissions from energy generation. *Environ. Sci. Technol.* **2000**, *34*, 3051–3057. [CrossRef]

52. Jiries, A.G.; Hussein, H.H.; Lintelmann, J. Polycyclic aromatic hydrocarbon in rain and street runoff in Amman, Jordan. *J. Environ. Sci.* **2003**, *15*, 848–853.

53. Forsgren, A.J. *Wastewater Treatment: Occurrence and Fate of Polycyclic Aromatic Hydrocarbons (PAHs)*, 1st ed.; CRC Press: Boca Raton, FL, USA, 2015. [CrossRef]

54. Huang, H.; Buekens, A. Chlorinated dioxins and furans as trace products of combustion: Some theoretical aspects. *Toxicol. Environ. Chem.* **2000**, *74*, 179–193. [CrossRef]

55. Novotna, B.; Topinka, J.; Solansky, I.; Chvatalova, I.; Lnenickova, Z.; Sram, R.J. Impact of air pollution and genotype variability on DNA damage in Prague policemen. *Toxicol. Lett.* **2007**, *172*, 37–47. [CrossRef] [PubMed]

56. Batarseh, M.I.; Kreuzig, R.; Bahadir, M. Residue analysis of organic pollutants in sediments from the Amman/Zarqa area in Jordan. Part 1: Development of analytical methods and distribution patterns of PAHs. *Fresenius Environ. Bull.* **2003**, *12*, 972–978.

57. Majumdar, D.; Rajaram, B.; Meshram, S.; Suryawanshi, P.; Chalapati Rao, C.V. Worldwide distribution of polyclyclic aromatic hydrocarbons in urban road dust. *Int. J. Environ. Sci. Technol.* **2016**, *14*, 397–420. [CrossRef]

58. Jiries, A.; Hussain, H.; Lintelmann, J. Determination of polycyclic aromatic hydrocarbons in wastewater, sediments, sludge and plants in Karak Province, Jordan. *Water Air Soil Pollut.* **2000**, *121*, 217–228. [CrossRef]

59. Tian, W.; Bai, J.; Liu, K.; Sun, H.; Zhao, Y. Occurrence and removal of polycyclic aromatic hydrocarbons in the wastewater treatment process. *Ecotoxicol. Environ. Saf.* **2012**, *82*, 1–7. [CrossRef]

60. Wang, X.; Xi, B.; Huo, S.; Sun, W.; Pan, H.; Zhang, J.; Ren, Y.; Liu, H. Characterization, treatment and releases of PBDEs and PAHs in a typical municipal sewage treatment plant situated beside an urban river, East China. *J. Environ. Sci.* **2013**, *25*, 1281–1290. [CrossRef]

61. Sun, H.M.; Tian, W.J.; Wang, Y.M. Occurrence and fate of polycyclic aromatic hydrocarbons in the anaerobic-anoxic-oxic wastewater treatment process. *Adv. Mater. Res.* **2012**, *610–613*, 1722–1725. [CrossRef]

62. Jia, C.; Batterman, S. A critical review of naphthalene sources and exposures relevant to indoor and outdoor air. *Int. J. Environ. Res. Public. Health* **2010**, *7*, 2903–2939. [CrossRef]

63. Robles, H. Naphthalene. In *Encyclopedia of Toxicology*; Wexler, P., Ed.; Academic Press: Oxford, UK, 2014; pp. 437–439. [CrossRef]

64. Sudakin, D.L.; Stone, D.L.; Power, L. Naphthalene mothballs: Emerging and recurring issues and their relevance to environmental health. *Curr. Top. Toxicol.* **2011**, *7*, 13–19. [PubMed]

65. Arizavi, A.; Mirbagheri, N.S.; Hosseini, Z.; Chen, P.; Sabbaghi, S. Efficient removal of naphthalene from aqueous solutions using a nanoporous kaolin/Fe_3O_4 composite. *Int. J. Environ. Sci. Technol.* **2020**, *17*, 1991–2002. [CrossRef]

66. Nesterenko-Malkovskaya, A.; Kirzhner, F.; Zimmels, Y.; Armon, R. Eichhornia crassipes capability to remove naphthalene from wastewater in the absence of bacteria. *Chemosphere* **2012**, *87*, 1186–1191. [CrossRef]

67. Pereira, L.; Alves, M. Dyes—Environmental impact and remediation. In *Environmental Protection Strategies for Sustainable Development*; Malik, A., Grohmann, E., Eds.; Springer: Dordrecht, The Netherlands, 2012; pp. 111–162. [CrossRef]

68. Hunger, K.; Gregory, P.; Miederer, P.; Berneth, H.; Heid, C.; Mennicke, W. Important chemical chromophores of dye classes. In *Industrial Dyes, Hunger, K., Ed.*; John Wiley & Sons Inc.: Hoboken, NJ, USA, 2002; pp. 13–112. [CrossRef]

69. Benkhaya, S.; M' rabet, S.; El Harfi, A. A review on classifications, recent synthesis and applications of textile dyes. *Inorg. Chem. Commun.* **2020**, *115*, 107891. [CrossRef]

70. Berradi, M.; Hsissou, R.; Khudhair, M.; Assouag, M.; Cherkaoui, O.; El Bachiri, A.; El Harfi, A. Textile finishing dyes and their impact on aquatic environs. *Heliyon* **2019**, *5*, e02711. [CrossRef] [PubMed]

71. Forgacs, E.; Cserháti, T.; Oros, G. Removal of synthetic dyes from wastewaters: A review. *Environ. Int.* **2004**, *30*, 953–971. [CrossRef]

72. Yan, J.; Wang, L.; Fu, P.P.; Yu, H. Photomutagenicity of 16 polycyclic aromatic hydrocarbons from the US EPA priority pollutant list. *Mutat. Res. Genet. Toxicol. Environ. Mutagen.* **2004**, *557*, 99–108. [CrossRef]

73. Ravindra, K.; Sokhi, R.; Van Grieken, R. Atmospheric polycyclic aromatic hydrocarbons: Source attribution, emission factors and regulation. *Atmos. Environ.* **2008**, *42*, 2895–2921. [CrossRef]

74. Ghodke, S.A.; Sonawane, S.H.; Bhanvase, B.A.; Potoroko, I. Advanced engineered nanomaterials for the treatment of wastewater. In *Handbook of Nanomaterials for Industrial Applications*; Mustansar Hussain, C., Ed.; Elsevier: Amsterdam, The Netherlands, 2018; pp. 959–970. [CrossRef]

75. Naushad, M.; Alqadami, A.A.; AlOthman, Z.A.; Alsohaimi, I.H.; Algamdi, M.S.; Aldawsari, A.M. Adsorption kinetics, isotherm and reusability studies for the removal of cationic dye from aqueous medium using arginine modified activated carbon. *J. Mol. Liq.* **2019**, *293*, 111442. [CrossRef]

76. Kadirvelu, K.; Kavipriya, M.; Karthika, C.; Radhika, M.; Vennilamani, N.; Pattabhi, S. Utilization of various agricultural wastes for activated carbon preparation and application for the removal of dyes and metal ions from aqueous solutions. *Bioresour. Technol.* **2003**, *87*, 129–132. [CrossRef]

77. Katheresan, V.; Kansedo, J.; Lau, S.Y. Efficiency of various recent wastewater dye removal methods: A review. *J. Environ. Chem. Eng.* **2018**, *6*, 4676–4697. [CrossRef]

78. Pai, S.; Kini, M.S.; Selvaraj, R. A review on adsorptive removal of dyes from wastewater by hydroxyapatite nanocomposites. *Environ. Sci. Pollut. Res. Int.* **2019**. [CrossRef]

79. Kiriakidou, F.; Kondarides, D.I.; Verykios, X.E. The effect of operational parameters and TiO_2-doping on the photocatalytic degradation of azo-dyes. *Catal. Today* **1999**, *54*, 119–130. [CrossRef]

80. Adeola, A.O.; Forbes, P.B.C. Advances in water treatment technologies for removal of polycyclic aromatic hydrocarbons: Existing concepts, emerging trends, and future prospects. *Water Environ. Res.* **2020**. [CrossRef]

81. Amin, M.T.; Alazba, A.A.; Manzoor, U. A review of removal of pollutants from water/wastewater using different types of nanomaterials. *Adv. Mater. Sci. Eng.* **2014**, *2014*, 1–24. [CrossRef]

82. Hlongwane, G.N.; Sekoai, P.T.; Meyyappan, M.; Moothi, K. Simultaneous removal of pollutants from water using nanoparticles: A shift from single pollutant control to multiple pollutant control. *Sci. Total Environ.* **2019**, *656*, 808–833. [CrossRef] [PubMed]

83. Rajasekhar, B.; Nambi, I.M.; Govindarajan, S.K. Investigating the degradation of nC_{12} to nC_{23} alkanes and PAHs in petroleum-contaminated water by electrochemical advanced oxidation process using an inexpensive $Ti/Sb-SnO_2/PbO_2$ anode. *Chem. Eng. J.* **2021**, *404*, 125268. [CrossRef]

84. Singa, P.K.; Isa, M.H.; Lim, J.W.; Ho, Y.C.; Krishnan, S. Photo-Fenton process for removal of polycyclic aromatic hydrocarbons from hazardous waste landfill leachate. *Int. J. Environ. Sci. Technol.* **2020**. [CrossRef]

85. Wilson, S.C.; Jones, K.C. Bioremediation of soil contaminated with polynuclear aromatic hydrocarbons (PAHs): A review. *Environ. Pollut.* **1993**, *81*, 229–249. [CrossRef]

86. Manariotis, I.D.; Karapanagioti, H.K.; Chrysikopoulos, C.V. Degradation of PAHs by high frequency ultrasound. *Water Res.* **2011**, *45*, 2587–2594. [CrossRef]

87. Khulbe, K.C.; Matsuura, T. Removal of heavy metals and pollutants by membrane adsorption techniques. *Appl. Water Sci.* **2018**, *8*, 19. [CrossRef]

88. Trojanowicz, M. Removal of persistent organic pollutants (POPs) from waters and wastewaters by the use of ionizing radiation. *Sci. Total. Environ.* **2020**, *718*, 134425. [CrossRef] [PubMed]

89. Zhang, W.; Wei, C.; An, G. Distribution, partition and removal of polycyclic aromatic hydrocarbons (PAHs) during coking wastewater treatment processes. *Environ. Sci. Process Impacts* **2015**, *17*, 975–984. [CrossRef]

90. Fatone, F.; Di Fabio, S.; Bolzonella, D.; Cecchi, F. Fate of aromatic hydrocarbons in Italian municipal wastewater systems: An overview of wastewater treatment using conventional activated-sludge processes (CASP) and membrane bioreactors (MBRs). *Water Res.* **2011**, *45*, 93–104. [CrossRef]

91. Zhu, X.; Ni, J.; Lai, P. Advanced treatment of biologically pretreated coking wastewater by electrochemical oxidation using boron-doped diamond electrodes. *Water Res.* **2009**, *43*, 4347–4355. [CrossRef] [PubMed]

92. Sakulthaew, C.; Comfort, S.; Chokejaroenrat, C.; Harris, C.; Li, X. A combined chemical and biological approach to transforming and mineralizing PAHs in runoff water. *Chemosphere* **2014**, *117*, 1–9. [CrossRef]

93. Anjum, M.; Miandad, R.; Waqas, M.; Gehany, F.; Barakat, M.A. Remediation of wastewater using various nano-materials. *Arab. J. Chem.* **2019**, *12*, 4897–4919. [CrossRef]

94. Wacławek, S.; Padil, V.V.T.; Černík, M. Major advances and challenges in heterogeneous catalysis for environmental applications: A review. *Ecol. Chem. Eng. S* **2018**, *25*, 9–34. [CrossRef]

95. Rasalingam, S.; Peng, R.; Koodali, R.T. Removal of hazardous pollutants from wastewaters: Applications of TiO$_2$-SiO$_2$ mixed oxide materials. *J. Nanomater.* **2014**, *2014*, 1–42. [CrossRef]

96. Crini, G.; Lichtfouse, E. Advantages and disadvantages of techniques used for wastewater treatment. *Environ. Chem. Lett.* **2019**, *17*, 145–155. [CrossRef]

97. Oturan, M.A.; Aaron, J.-J. Advanced oxidation processes in water/wastewater treatment: Principles and applications. A review. *Crit. Rev. Env. Sci. Tec.* **2014**, *44*, 2577–2641. [CrossRef]

98. Lee, S.-Y.; Park, S.-J. TiO$_2$ photocatalyst for water treatment applications. *J. Ind. Eng. Chem.* **2013**, *19*, 1761–1769. [CrossRef]

99. Mousavi, M.; Habibi-Yangjeh, A.; Pouran, S.R. Review on magnetically separable graphitic carbon nitride-based nanocomposites as promising visible-light-driven photocatalysts. *J. Mater. Sci. Mater. Electron.* **2018**, *29*, 1719–1747. [CrossRef]

100. Mokhbi, Y.; Korichi, M.; Akchiche, Z. Combined photocatalytic and Fenton oxidation for oily wastewater treatment. *Appl. Water Sci.* **2019**, *9*, 35. [CrossRef]

101. Ramadan, W.; Dillert, R.; Koch, J.; Tegenkamp, C.; Bahnemann, D.W. Changes in the solid-state properties of bismuth iron oxide during the photocatalytic reformation of formic acid. *Catal. Today* **2019**, *326*, 22–29. [CrossRef]

102. AlSalka, Y.; Granone, L.I.; Ramadan, W.; Hakki, A.; Dillert, R.; Bahnemann, D.W. Iron-based photocatalytic and photoelectrocatalytic nano-structures: Facts, perspectives, and expectations. *Appl. Catal. B* **2019**, *244*, 1065–1095. [CrossRef]

103. Raza, W.; Haque, M.M.; Muneer, M.; Bahnemann, D. Synthesis of visible light driven TiO$_2$ coated carbon nanospheres for degradation of dyes. *Arab. J. Chem.* **2019**, *12*, 3534–3545. [CrossRef]

104. Al-Madanat, O.; AlSalka, Y.; Curti, M.; Dillert, R.; Bahnemann, D.W. Mechanistic insights into hydrogen evolution by photocatalytic reforming of naphthalene. *ACS Catal.* **2020**, *10*, 7398–7412. [CrossRef]

105. AlSalka, Y.; Al-Madanat, O.; Curti, M.; Hakki, A.; Bahnemann, D.W. Photocatalytic H$_2$ evolution from oxalic acid: Effect of cocatalysts and carbon dioxide radical anion on the surface charge transfer mechanisms. *ACS Appl. Energy Mater.* **2020**, *3*, 6678–6691. [CrossRef]

106. Megatif, L.; Dillert, R.; Bahnemann, D.W. Reaction rate study of the photocatalytic degradation of dichloroacetic acid in a black body reactor. *Catalysts* **2019**, *9*, 635. [CrossRef]

107. Faycal Atitar, M.; Ismail, A.A.; Dillert, R.; Bahnemann, D.W. Photodegradation of herbicide imazapyr and phenol over mesoporous bicrystalline phases TiO$_2$: A Kinetic study. *Catalysts* **2019**, *9*, 640. [CrossRef]

108. Jagadale, T.; Kulkarni, M.; Pravarthana, D.; Ramadan, W.; Thakur, P. Photocatalytic degradation of azo dyes using Au:TiO$_2$, gamma-Fe$_2$O$_3$:TiO$_2$ functional nanosystems. *J. Nanosci. Nanotechnol.* **2012**, *12*, 928–936. [CrossRef]

109. Fox, M.A.; Dulay, M.T. Heterogeneous photocatalysis. *Chem. Rev.* **1993**, *93*, 341–357. [CrossRef]

110. Schneider, J.; Matsuoka, M.; Takeuchi, M.; Zhang, J.; Horiuchi, Y.; Anpo, M.; Bahnemann, D.W. Understanding TiO$_2$ photocatalysis: Mechanisms and materials. *Chem. Rev.* **2014**, *114*, 9919–9986. [CrossRef] [PubMed]

111. Shayegan, Z.; Lee, C.-S.; Haghighat, F. TiO$_2$ photocatalyst for removal of volatile organic compounds in gas phase—A review. *Chem. Eng. J.* **2018**, *334*, 2408–2439. [CrossRef]

112. Pelaez, M.; Nolan, N.T.; Pillai, S.C.; Seery, M.K.; Falaras, P.; Kontos, A.G.; Dunlop, P.S.M.; Hamilton, J.W.J.; Byrne, J.A.; O'Shea, K.; et al. A review on the visible light active titanium dioxide photocatalysts for environmental applications. *Appl. Catal. B* **2012**, *125*, 331–349. [CrossRef]

113. Choquette-Labbé, M.; Shewa, W.; Lalman, J.; Shanmugam, S. Photocatalytic degradation of phenol and phenol derivatives using a nano-TiO$_2$ catalyst: Integrating quantitative and qualitative factors using response surface methodology. *Water* **2014**, *6*, 1785–1806. [CrossRef]

114. Kamat, P.V. Meeting the clean energy demand: Nanostructure architectures for solar energy conversion. *J. Phys. Chem. C* **2007**, *111*, 2834–2860. [CrossRef]

115. Etacheri, V.; Di Valentin, C.; Schneider, J.; Bahnemann, D.; Pillai, S.C. Visible-light activation of TiO$_2$ photocatalysts: Advances in theory and experiments. *J. Photochem. Photobiol. C* **2015**, *25*, 1–29. [CrossRef]

116. Rachna; Rani, M.; Shanker, U. Sunlight mediated improved photocatalytic degradation of carcinogenic benz[a]anthracene and benzo[a]pyrene by zinc oxide encapsulated hexacyanoferrate nanocomposite. *J. Photochem. Photobiol. A* **2019**, *381*, 111861. [CrossRef]

117. Fu, J.; Kyzas, G.Z.; Cai, Z.; Deliyanni, E.A.; Liu, W.; Zhao, D. Photocatalytic degradation of phenanthrene by graphite oxide-TiO$_2$-Sr(OH)$_2$/SrCO$_3$ nanocomposite under solar irradiation: Effects of water quality parameters and predictive modeling. *Chem. Eng. J.* **2018**, *335*, 290–300. [CrossRef]

118. El-Mekkawi, D.M.; Abdelwahab, N.A.; Mohamed, W.A.A.; Taha, N.A.; Abdel-Mottaleb, M.S.A. Solar photocatalytic treatment of industrial wastewater utilizing recycled polymeric disposals as TiO$_2$ supports. *J. Clean. Prod.* **2020**, *249*, 119430. [CrossRef]

119. Horikoshi, S.; Serpone, N. Can the photocatalyst TiO$_2$ be incorporated into a wastewater treatment method? Background and prospects. *Catal. Today* **2020**, *340*, 334–346. [CrossRef]

120. Zhai, S.; Zhu, G.; Wei, X.; Ge, M. Enhanced catalytic degradation of polyvinyl alcohol from aqueous solutions by novel synthesis of MnCoO$_3$@γ-Al$_2$O$_3$ nanocomposites: Performance, degradation intermediates and mechanism. *J. Mol. Liq.* **2021**, *323*, 114569. [CrossRef]

121. Sola, A.C.; Ramírez de la Piscina, P.; Homs, N. Behaviour of Pt/TiO$_2$ catalysts with different morphological and structural characteristics in the photocatalytic conversion of ethanol aqueous solutions. *Catal. Today* **2020**, *341*, 13–20. [CrossRef]

122. Ivanova, I.; Schneider, J.; Gutzmann, H.; Kliemann, J.-O.; Gärtner, F.; Klassen, T.; Bahnemann, D.; Mendive, C.B. Photocatalytic degradation of oxalic and dichloroacetic acid on TiO$_2$ coated metal substrates. *Catal. Today* **2013**, *209*, 84–90. [CrossRef]

123. Hasan, I.; Shekhar, C.; Bin, S., II; Khan, R.A.; Alsalme, A. Ecofriendly green synthesis of the ZnO-doped CuO@Alg bionanocomposite for efficient oxidative degradation of p-nitrophenol. *ACS Omega* **2020**, *5*, 32011–32022. [CrossRef]

124. Wu, S.; Li, X.; Tian, Y.; Lin, Y.; Hu, Y.H. Excellent photocatalytic degradation of tetracycline over black anatase-TiO$_2$ under visible light. *Chem. Eng. J.* **2021**, *406*, 126747. [CrossRef]

125. Miao, Y.; Xu, X.; Liu, K.; Yu, S.; Wang, Y.; Yang, S. Preparation and activity evaluation of the novel Cu/TiO$_2$ nanometer photocatalytic materials. *Sci. Adv. Mater.* **2020**, *12*, 1027–1033. [CrossRef]

126. Rani, M.; Shanker, U.; Yadav, J.; Keshu. Degradation of pesticides residue by engineered nanomaterials. In *Sustainable Agriculture Reviews 48*; Inamuddin, Ahamed, M.I., Lichtfouse, E., Eds.; Springer International Publishing: Cham, Switzerland, 2021; pp. 259–310. [CrossRef]

127. Park, H.; Kim, H.-i.; Moon, G.-h.; Choi, W. Photoinduced charge transfer processes in solar photocatalysis based on modified TiO$_2$. *Energy Environ. Sci.* **2016**, *9*, 411–433. [CrossRef]

128. Kumaravel, V.; Mathew, S.; Bartlett, J.; Pillai, S.C. Photocatalytic hydrogen production using metal doped TiO$_2$: A review of recent advances. *Appl. Catal. B* **2019**, *244*, 1021–1064. [CrossRef]

129. Pellegrino, F.; Sordello, F.; Mino, L.; Minero, C.; Hodoroaba, V.-D.; Martra, G.; Maurino, V. Formic acid photoreforming for hydrogen production on shap-controlled anatase TiO$_2$ nanoparticles: Assessment of the role of fluorides, {101}/{001} surfaces ratio, and platinization. *ACS Catal.* **2019**, *9*, 6692–6697. [CrossRef]

130. Kampouri, S.; Stylianou, K.C. Dual-functional photocatalysis for simultaneous hydrogen production and oxidation of organic substances. *ACS Catal.* **2019**, *9*, 4247–4270. [CrossRef]

131. AlSalka, Y.; Hakki, A.; Fleisch, M.; Bahnemann, D.W. Understanding the degradation pathways of oxalic acid in different photocatalytic systems: Towards simultaneous photocatalytic hydrogen evolution. *J. Photochem. Photobiol. A* **2018**, *366*, 81–90. [CrossRef]

132. Hakki, A.; AlSalka, Y.; Mendive, C.B.; Ubogui, J.; dos Santos Claro, P.C.; Bahnemann, D. Hydrogen production by heterogeneous photocatalysis. In *Encyclopedia of Interfacial Chemistry*; Wandelt, K., Ed.; Elsevier: Oxford, UK, 2018; pp. 413–419. [CrossRef]

133. Sivula, K.; Van De Krol, R. Semiconducting materials for photoelectrochemical energy conversion. *Nat. Rev. Mater.* **2016**, *1*, 15010. [CrossRef]

134. Takanabe, K.; Domen, K. Toward visible light response: Overall water splitting using heterogeneous photocatalysts. *Green* **2011**, *1*, 313–322. [CrossRef]

135. Maeda, K.; Domen, K. Photocatalytic water splitting: Recent progress and future challenges. *J. Phys. Chem. Lett.* **2010**, *1*, 2655–2661. [CrossRef]

136. Cao, W. *Semiconductor Photocatalysis: Materials, Mechanisms and Applications*; InTech: Rijeka, Croatia, 2016. [CrossRef]

137. Jiang, C.; Moniz, S.J.; Wang, A.; Zhang, T.; Tang, J. Photoelectrochemical devices for solar water splitting–materials and challenges. *Chem. Soc. Rev.* **2017**, *46*, 4645–4660. [CrossRef]

138. Kisch, H. *Semiconductor Photocatalysis Principle and Applications*; Wiley-VCH: Hoboken, NJ, USA, 2015.

139. Friehs, E.; AlSalka, Y.; Jonczyk, R.; Lavrentieva, A.; Jochums, A.; Walter, J.-G.; Stahl, F.; Scheper, T.; Bahnemann, D. Toxicity, phototoxicity and biocidal activity of nanoparticles employed in photocatalysis. *J. Photochem. Photobiol. C* **2016**, *29*, 1–28. [CrossRef]

140. Hernández-Ramírez, A.; Medina-Ramírez, I. Semiconducting materials. In *Photocatalytic Semiconductors*; Hernández-Ramírez, A., Medina-Ramírez, I., Eds.; Springer International Publishing: Cham, Switzerland, 2015; pp. 1–40. [CrossRef]

141. Barr, A. Electrical properties of semiconductors. In *Electronic Materials*; Miller, L.S., Mullin, J.B., Eds.; Springer: Boston, MA, USA, 1991; pp. 19–24. [CrossRef]

142. Fonash, S.J. Structures, materials, and scale. In *Solar Cell Device Physics*; Fonash, S.J., Ed.; Academic Press: Boston, MA, USA, 2010; pp. 67–120. [CrossRef]

143. Hoffmann, M.R.; Martin, S.T.; Choi, W.; Bahnemann, D.W. Environmental applications of semiconductor photocatalysis. *Chem. Rev.* **1995**, *95*, 69–96. [CrossRef]

144. Mills, A.; Le Hunte, S. An overview of semiconductor photocatalysis. *J. Photochem. Photobiol. A* **1997**, *108*, 1–35. [CrossRef]

145. Linsebigler, A.L.; Lu, G.; Yates, J.T., Jr. Photocatalysis on TiO_2 surfaces: Principles, mechanisms, and selected results. *Chem. Rev.* **1995**, *95*, 735–758. [CrossRef]

146. Wang, F.; Li, Q.; Xu, D. Recent progress in semiconductor-based nanocomposite photocatalysts for solar-to-chemical energy conversion. *Adv. Energy Mater.* **2017**, *7*, 1700529. [CrossRef]

147. Takanabe, K. Photocatalytic water splitting: Quantitative approaches toward photocatalyst by design. *ACS Catal.* **2017**, *7*, 8006–8022. [CrossRef]

148. Peter, L.M. Photoelectrochemistry: From basic principles to photocatalysis. In *Photocatalysis: Fundamentals and Perspectives*; The Royal Society of Chemistry: London, UK, 2016; pp. 1–28.

149. Habisreutinger, S.N.; Schmidt-Mende, L.; Stolarczyk, J.K. Photocatalytic reduction of CO_2 on TiO_2 and other semiconductors. *Angew. Chem. Int. Ed.* **2013**, *52*, 7372–7408. [CrossRef]

150. AlSalka, Y.; Hakki, A.; Schneider, J.; Bahnemann, D.W. Co-catalyst-free photocatalytic hydrogen evolution on TiO_2: Synthesis of optimized photocatalyst through statistical material science. *Appl. Catal. B* **2018**, *238*, 422–433. [CrossRef]

151. Walter, M.G.; Warren, E.L.; McKone, J.R.; Boettcher, S.W.; Mi, Q.; Santori, E.A.; Lewis, N.S. Solar water splitting cells. *Chem. Rev.* **2010**, *110*, 6446–6473. [CrossRef] [PubMed]

152. Walter, M.G.; Warren, E.L.; McKone, J.R.; Boettcher, S.W.; Mi, Q.; Santori, E.A.; Lewis, N.S. Correction to solar water splitting cells. *Chem. Rev.* **2011**, *111*, 5815. [CrossRef]

153. Pichat, P. A brief overview of photocatalytic mechanisms and pathways in water. *Water Sci. Technol.* **2007**, *55*, 167–173. [CrossRef]

154. Ni, M.; Leung, M.K.; Leung, D.Y.; Sumathy, K. A review and recent developments in photocatalytic water-splitting using TiO_2 for hydrogen production. *Renew. Sust. Energ. Rev.* **2007**, *11*, 401–425. [CrossRef]

155. Schneider, J.; Kandiel, T.A.; Bahnemann, D.W. Solar photocatalytic hydrogen production: Current status and future challenges. In *Materials and Processes for Solar Fuel Production*; Viswanathan, B., Subramanian, V., Lee, J.S., Eds.; Springer: New York, NY, USA, 2014; pp. 41–74. [CrossRef]

156. Cho, Y.J.; Moon, G.H.; Kanazawa, T.; Maeda, K.; Choi, W. Selective dual-purpose photocatalysis for simultaneous H_2 evolution and mineralization of organic compounds enabled by a Cr_2O_3 barrier layer coated on $Rh/SrTiO_3$. *Chem. Commun.* **2016**, *52*, 9636–9639. [CrossRef]

157. Shimura, K.; Yoshida, H. Heterogeneous photocatalytic hydrogen production from water and biomass derivatives. *Energy Environ. Sci.* **2011**, *4*, 2467–2481. [CrossRef]

158. Jeon, T.H.; Koo, M.S.; Kim, H.; Choi, W. Dual-functional photocatalytic and photoelectrocatalytic systems for energy- and resource-recovering water treatment. *ACS Catal.* **2018**, *8*, 11542–11563. [CrossRef]

159. Ohtani, B. Photocatalysis A to Z—What we know and what we do not know in a scientific sense. *J. Photochem. Photobiol. C* **2010**, *11*, 157–178. [CrossRef]

160. Balayeva, N.O.; Zheng, N.; Dillert, R.; Bahnemann, D.W. Visible-light-mediated photocatalytic aerobic dehydrogenation of N-heterocycles by surface-grafted TiO_2 and 4-amino-TEMPO. *ACS Catal.* **2019**, *9*, 10694–10704. [CrossRef]

161. Zhang, L.; Jiang, D.; Irfan, R.M.; Tang, S.; Chen, X.; Du, P. Highly efficient and selective photocatalytic dehydrogenation of benzyl alcohol for simultaneous hydrogen and benzaldehyde production over Ni-decorated $Zn_{0.5}Cd_{0.5}S$ solid solution. *J. Energy Chem.* **2019**, *30*, 71–77. [CrossRef]

162. Zheng, Y.W.; Chen, B.; Ye, P.; Feng, K.; Wang, W.; Meng, Q.Y.; Wu, L.Z.; Tung, C.H. Photocatalytic hydrogen-evolution cross-couplings: Benzene C-H amination and hydroxylation. *J. Am. Chem. Soc.* **2016**, *138*, 10080–10083. [CrossRef]

163. Puga, A.V. Photocatalytic production of hydrogen from biomass-derived feedstocks. *Coord. Chem. Rev.* **2016**, *315*, 1–66. [CrossRef]

164. Schneider, J.; Bahnemann, D.W. Undesired role of sacrificial reagents in photocatalysis. *J. Phys. Chem. Lett.* **2013**, *4*, 3479–3483. [CrossRef]

165. Chen, X.; Shen, S.; Guo, L.; Mao, S.S. Semiconductor-based photocatalytic hydrogen generation. *Chem. Rev.* **2010**, *110*, 6503–6570. [CrossRef]

166. Kandiel, T.A.; Ivanova, I.; Bahnemann, D.W. Long-term investigation of the photocatalytic hydrogen production on platinized TiO_2: An isotopic study. *Energy Environ. Sci.* **2014**, *7*, 1420–1425. [CrossRef]

167. Al-Madanat, O.; AlSalka, Y.; Dillert, R.; Bahnemann, D. Photocatalytic H_2 production from naphthalene by various TiO_2 photocatalysts: Impact of Pt loading and formation of intermediates. *Catalysts* **2021**, *11*, 107. [CrossRef]

168. Bahruji, H.; Bowker, M.; Davies, P.R.; Morgan, D.J.; Morton, C.; Egerton, T.; Kennedy, J.; Jones, W. Rutile TiO_2–Pd photocatalysts for hydrogen gas production from methanol reforming. *Top. Catal.* **2015**, *58*, 70–76. [CrossRef]

169. Ismail, A.A.; Robben, L.; Bahnemann, D.W. Study of the efficiency of UV and visible-light photocatalytic oxidation of methanol on mesoporous RuO_2–TiO_2 nanocomposites. *ChemPhysChem* **2011**, *12*, 982–991. [CrossRef] [PubMed]

170. Prairie, M.R.; Evans, L.R.; Stange, B.M.; Martinez, S.L. An investigation of titanium dioxide photocatalysis for the treatment of water contaminated with metals and organic chemicals. *Environ. Sci. Technol.* **1993**, *27*, 1776–1782. [CrossRef]

171. Mo, S.D.; Ching, W.Y. Electronic and optical properties of three phases of titanium dioxide: Rutile, anatase, and brookite. *Phys. Rev. B* **1995**, *51*, 13023–13032. [CrossRef] [PubMed]

172. Enke, C.G. Nonstoichiometry, diffusion, and electrical conductivity in binary metal oxides. (Wiley series on the science and technology of materials). P. Kofstad. 160 Abb. 11 Table XI, 382 S. Ca. 1060 Schrifttumshinweise. Format 15.5 × 23 cm. Wiley Interscience (J. Wiley & Sons, Inc.) New York-London-Sydney-Toronto,1972. Gebunden ca. DM 52. *Werkst. Korros.* **1974**, *25*, 801–802. [CrossRef]

173. Chretien, S.; Metiu, H. Electronic structure of partially reduced rutile TiO_2 (110) surface: Where are the unpaired electrons located? *J. Phys. Chem. C* **2011**, *115*, 4696–4705. [CrossRef]

174. Diebold, U. The surface science of titanium dioxide. *Surf. Sci. Rep.* **2003**, *48*, 53–229. [CrossRef]

175. Qian, R.; Zong, H.; Schneider, J.; Zhou, G.; Zhao, T.; Li, Y.; Yang, J.; Bahnemann, D.W.; Pan, J.H. Charge carrier trapping, recombination and transfer during TiO_2 photocatalysis: An overview. *Catal. Today* **2019**, *335*, 78–90. [CrossRef]

176. Kohtani, S.; Kawashima, A.; Miyabe, H. Reactivity of trapped and accumulated electrons in titanium dioxide photocatalysis. *Catalysts* **2017**, *7*, 303. [CrossRef]

177. Serpone, N.; Lawless, D.; Khairutdinov, R. Size effects on the photophysical properties of colloidal anatase TiO_2 particles: Size quantization versus direct transitions in this indirect semiconductor? *J. Phys. Chem.* **1995**, *99*, 16646–16654. [CrossRef]

178. Stevanovic, A.; Yates Jr, J.T. Probe of NH_3 and CO adsorption on the very outermost surface of a porous TiO_2 adsorbent using photoluminescence spectroscopy. *Langmuir* **2012**, *28*, 5652–5659. [CrossRef] [PubMed]

179. Yoshihara, T.; Katoh, R.; Furube, A.; Tamaki, Y.; Murai, M.; Hara, K.; Murata, S.; Arakawa, H.; Tachiya, M. Identification of reactive species in photoexcited nanocrystalline TiO_2 films by wide-wavelength-range (400−2500 nm) transient absorption spectroscopy. *J. Phys. Chem. B* **2004**, *108*, 3817–3823. [CrossRef]

180. Howe, R.F.; Gratzel, M. EPR study of hydrated anatase under UV irradiation. *J. Phys. Chem.* **1987**, *91*, 3906–3909. [CrossRef]

181. Howe, R.F.; Gratzel, M. EPR observation of trapped electrons in colloidal titanium dioxide. *J. Phys. Chem.* **1985**, *89*, 4495–4499. [CrossRef]

182. Wu, C.-Y.; Tu, K.-J.; Deng, J.-P.; Lo, Y.-S.; Wu, C.-H. Markedly enhanced surface hydroxyl groups of TiO_2 nanoparticles with superior water-dispersibility for photocatalysis. *Materials* **2017**, *10*, 566. [CrossRef]

183. Augustynski, J. The role of the surface intermediates in the photoelectrochemical behaviour of anatase and rutile TiO_2. *Electrochim. Acta* **1993**, *38*, 43–46. [CrossRef]

184. Zhang, J.; Zhou, P.; Liu, J.; Yu, J. New understanding of the difference of photocatalytic activity among anatase, rutile and brookite TiO_2. *PCCP* **2014**, *16*, 20382–20386. [CrossRef]

185. Sachs, M.; Pastor, E.; Kafizas, A.; Durrant, J.R. Evaluation of surface state mediated charge recombination in anatase and rutile TiO_2. *J. Phys. Chem. Lett.* **2016**, *7*, 3742–3746. [CrossRef] [PubMed]

186. Knorr, F.J.; Mercado, C.C.; McHale, J.L. Trap-state distributions and carrier transport in pure and mixed-phase TiO_2: Influence of contacting solvent and interphasial electron transfer. *J. Phys. Chem. C* **2008**, *112*, 12786–12794. [CrossRef]

187. Wang, X.; Feng, Z.; Shi, J.; Jia, G.; Shen, S.; Zhou, J.; Li, C. Trap states and carrier dynamics of TiO_2 studied by photoluminescence spectroscopy under weak excitation condition. *PCCP* **2010**, *12*, 7083–7090. [CrossRef] [PubMed]

188. Wang, X.; Kafizas, A.; Li, X.; Moniz, S.J.A.; Reardon, P.J.T.; Tang, J.; Parkin, I.P.; Durrant, J.R. Transient absorption spectroscopy of anatase and rutile: The impact of morphology and phase on photocatalytic activity. *J. Phys. Chem. C* **2015**, *119*, 10439–10447. [CrossRef]

189. Kim, W.; Tachikawa, T.; Moon, G.H.; Majima, T.; Choi, W. Molecular-level understanding of the photocatalytic activity difference between anatase and rutile nanoparticles. *Angew. Chem. Int. Ed.* **2014**, *53*, 14036–14041. [CrossRef]

190. Schindler, K.M.; Kunst, M. Charge-carrier dynamics in titania powders. *J. Phys. Chem.* **1990**, *94*, 8222–8226. [CrossRef]

191. Hurum, D.C.; Agrios, A.G.; Gray, K.A.; Rajh, T.; Thurnauer, M.C. Explaining the enhanced photocatalytic activity of degussa P25 mixed-phase TiO_2 using EPR. *J. Phys. Chem. B* **2003**, *107*, 4545–4549. [CrossRef]

192. Choi, W.; Termin, A.; Hoffmann, M.R. The role of metal ion dopants in quantum-sized TiO_2: Correlation between photoreactivity and charge carrier recombination dynamics. *J. Phys. Chem.* **1994**, *98*, 13669–13679. [CrossRef]

193. Asahi, R.; Morikawa, T.; Ohwaki, T.; Aoki, K.; Taga, Y. Visible-light photocatalysis in nitrogen-doped titanium oxides. *Science* **2001**, *293*, 269–271. [CrossRef]

194. Weber, M.F.; Dignam, M.J. Efficiency of splitting water with semiconducting photoelectrodes. *J. Electrochem. Soc.* **1984**, *131*, 1258–1265. [CrossRef]

195. Bahnemann, D.; Henglein, A.; Lilie, J.; Spanhel, L. Flash photolysis observation of the absorption spectra of trapped positive holes and electrons in colloidal titanium dioxide. *J. Phys. Chem.* **1984**, *88*, 709–711. [CrossRef]

196. Erdey-Grúz, T.; Volmer, M. Zur theorie der wasserstoff überspannung. *Z. Phys. Chem.* **1930**, *150*, 203–213. [CrossRef]

197. Kasarevic-Popovic, Z.; Behar, D.; Rabani, J. Role of excess electrons in TiO_2 nanoparticles coated with Pt in reduction reactions studied in radiolysis of aqueous solutions. *J. Phys. Chem. B* **2004**, *108*, 20291–20295. [CrossRef]

198. Hu, C.; Lv, C.; Liu, S.; Shi, Y.; Song, J.F.; Zhang, Z.; Cai, J.G.; Watanabe, A. Nickel phosphide electrocatalysts for hydrogen evolution reaction. *Catalysts* **2020**, *10*, 188. [CrossRef]

199. Michaelson, H.B. The work function of the elements and its periodicity. *J. Appl. Phys.* **1977**, *48*, 4729–4733. [CrossRef]

200. Xiong, G.; Shao, R.; Droubay, T.C.; Joly, A.G.; Beck, K.M.; Chambers, S.A.; Hess, W.P. Photoemission electron microscopy of TiO₂ anatase films embedded with rutile nanocrystals. *Adv. Funct. Mater.* **2007**, *17*, 2133–2138. [CrossRef]

201. Di Bartolomeo, A. Graphene Schottky diodes: An experimental review of the rectifying graphene/semiconductor heterojunction. *Phys. Rep.* **2016**, *606*, 1–58. [CrossRef]

202. Iwata, K.; Takaya, T.; Hamaguchi, H.-o.; Yamakata, A.; Ishibashi, T.-a.; Onishi, H.; Kuroda, H. Carrier dynamics in TiO₂ and Pt/TiO₂ powders observed by femtosecond time-resolved near-infrared spectroscopy at a spectral region of 0.9−1.5 μm with the direct absorption method. *J. Phys. Chem. B* **2004**, *108*, 20233–20239. [CrossRef]

203. Yamakata, A.; Ishibashi, T.-a.; Kato, H.; Kudo, A.; Onishi, H. Photodynamics of NaTaO₃ catalysts for efficient water splitting. *J. Phys. Chem. B* **2003**, *107*, 14383–14387. [CrossRef]

204. Yamakata, A.; Ishibashi, T.-A.; Onishi, H. Water-and oxygen-induced decay kinetics of photogenerated electrons in TiO₂ and Pt/TiO₂: A time-resolved infrared absorption study. *J. Phys. Chem. B* **2001**, *105*, 7258–7262. [CrossRef]

205. Fu, X.; Long, J.; Wang, X.; Leung, D.; Ding, Z.; Wu, L.; Zhang, Z.; Li, Z.; Fu, X. Photocatalytic reforming of biomass: A systematic study of hydrogen evolution from glucose solution. *Int. J. Hydrog. Energy* **2008**, *33*, 6484–6491. [CrossRef]

206. Jang, J.S.; Ji, S.M.; Bae, S.W.; Son, H.C.; Lee, J.S. Optimization of CdS/TiO₂ nano-bulk composite photocatalysts for hydrogen production from Na₂S/Na₂SO₃ aqueous electrolyte solution under visible light (λ ≥ 420 nm). *J. Photochem. Photobiol. A* **2007**, *188*, 112–119. [CrossRef]

207. Sabatier, P. Hydrogénations et déshydrogénations par catalyse. *Ber. Dtsch. Chem. Ges.* **1911**, *44*, 1984–2001. [CrossRef]

208. Trasatti, S. Work function, electronegativity, and electrochemical behaviour of metals: III. Electrolytic hydrogen evolution in acid solutions. *J. Electroanal. Chem. Interfacial Electrochem.* **1972**, *39*, 163–184. [CrossRef]

209. Nørskov, J.K.; Bligaard, T.; Logadottir, A.; Kitchin, J.; Chen, J.G.; Pandelov, S.; Stimming, U. Trends in the exchange current for hydrogen evolution. *J. Electrochem. Soc.* **2005**, *152*, J23–J26. [CrossRef]

210. Bamwenda, G.R.; Tsubota, S.; Nakamura, T.; Haruta, M. Photoassisted hydrogen production from a water-ethanol solution: A comparison of activities of Au-TiO₂ and Pt-TiO₂. *J. Photochem. Photobiol. A* **1995**, *89*, 177–189. [CrossRef]

211. Sheng, W.; Myint, M.; Chen, J.G.; Yan, Y. Correlating the hydrogen evolution reaction activity in alkaline electrolytes with the hydrogen binding energy on monometallic surfaces. *Energy Environ. Sci.* **2013**, *6*, 1509–1512. [CrossRef]

212. Naldoni, A.; D'Arienzo, M.; Altomare, M.; Marelli, M.; Scotti, R.; Morazzoni, F.; Selli, E.; Dal Santo, V. Pt and Au/TiO₂ photocatalysts for methanol reforming: Role of metal nanoparticles in tuning charge trapping properties and photoefficiency. *Appl. Catal. B* **2013**, *130–131*, 239–248. [CrossRef]

213. Park, H.; Reddy, D.A.; Kim, Y.; Lee, S.; Ma, R.; Kim, T.K. Synthesis of ultra-small palladium nanoparticles deposited on CdS nanorods by pulsed laser ablation in liquid: Role of metal nanocrystal size in the photocatalytic hydrogen production. *Chemistry* **2017**, *23*, 13112–13119. [CrossRef] [PubMed]

214. Wenderich, K.; Mul, G. Methods, mechanism, and applications of photodeposition in photocatalysis: A review. *Chem. Rev.* **2016**, *116*, 14587–14619. [CrossRef]

215. Pei, Z.; Weng, S.; Liu, P. Enhanced photocatalytic activity by bulk trapping and spatial separation of charge carriers: A case study of defect and facet mediated TiO₂. *Appl. Catal. B* **2016**, *180*, 463–470. [CrossRef]

216. Saravanan, R.; Gracia, F.; Stephen, A. Basic principles, mechanism, and challenges of photocatalysis. In *Nanocomposites for Visible Light-Induced Photocatalysis*; Khan, M.M., Pradhan, D., Sohn, Y., Eds.; Springer International Publishing: Cham, Switzerland, 2017; pp. 19–40. [CrossRef]

217. Al-Azri, Z.H.N.; Chen, W.-T.; Chan, A.; Jovic, V.; Ina, T.; Idriss, H.; Waterhouse, G.I.N. The roles of metal co-catalysts and reaction media in photocatalytic hydrogen production: Performance evaluation of M/TiO₂ photocatalysts (M = Pd, Pt, Au) in different alcohol–water mixtures. *J. Catal.* **2015**, *329*, 355–367. [CrossRef]

218. Al-Azri, Z.H.N.; AlOufi, M.; Chan, A.; Waterhouse, G.I.N.; Idriss, H. Metal particle size effects on the photocatalytic hydrogen ion reduction. *ACS Catal.* **2019**, *9*, 3946–3958. [CrossRef]

219. Bamwenda, G.R.; Tsubota, S.; Nakamura, T.; Haruta, M. The influence of the preparation methods on the catalytic activity of platinum and gold supported on TiO₂ for CO oxidation. *Catal. Lett.* **1997**, *44*, 83–87. [CrossRef]

220. Kozlova, E.A.; Lyubina, T.P.; Nasalevich, M.A.; Vorontsov, A.V.; Miller, A.V.; Kaichev, V.V.; Parmon, V.N. Influence of the method of platinum deposition on activity and stability of Pt/TiO₂ photocatalysts in the photocatalytic oxidation of dimethyl methylphosphonate. *Catal. Commun.* **2011**, *12*, 597–601. [CrossRef]

221. Marzun, G.; Streich, C.; Jendrzej, S.; Barcikowski, S.; Wagener, P. Adsorption of colloidal platinum nanoparticles to supports: Charge transfer and effects of electrostatic and steric interactions. *Langmuir* **2014**, *30*, 11928–11936. [CrossRef] [PubMed]

222. Wang, C.-y.; Pagel, R.; Bahnemann, D.W.; Dohrmann, J.K. Quantum yield of formaldehyde formation in the presence of colloidal TiO₂-based photocatalysts: Effect of intermittent illumination, platinization, and deoxygenation. *J. Phys. Chem. B* **2004**, *108*, 14082–14092. [CrossRef]

223. Haselmann, G.M.; Eder, D. Early-stage deactivation of platinum-loaded TiO₂ using in situ photodeposition during photocatalytic hydrogen evolution. *ACS Catal.* **2017**, *7*, 4668–4675. [CrossRef]

224. Li, F.B.; Li, X.Z. The enhancement of photodegradation efficiency using Pt–TiO₂ catalyst. *Chemosphere* **2002**, *48*, 1103–1111. [CrossRef]

225. Siuzdak, K.; Sawczak, M.; Klein, M.; Nowaczyk, G.; Jurga, S.; Cenian, A. Preparation of platinum modified titanium dioxide nanoparticles with the use of laser ablation in water. *Phys. Chem. Chem. Phys.* **2014**, *16*, 15199–15206. [CrossRef]

226. Murcia, J.J.; Navío, J.A.; Hidalgo, M.C. Insights towards the influence of Pt features on the photocatalytic activity improvement of TiO$_2$ by platinisation. *Appl. Catal. B* **2012**, *126*, 76–85. [CrossRef]

227. Farsinezhad, S.; Sharma, H.; Shankar, K. Interfacial band alignment for photocatalytic charge separation in TiO$_2$ nanotube arrays coated with CuPt nanoparticles. *Phys. Chem. Chem. Phys.* **2015**, *17*, 29723–29733. [CrossRef] [PubMed]

228. Wang, C.; Yin, L.; Zhang, L.; Liu, N.; Lun, N.; Qi, Y. Platinum-nanoparticle-modified TiO$_2$ nanowires with enhanced photocatalytic property. *ACS Appl. Mater. Interfaces* **2010**, *2*, 3373–3377. [CrossRef]

229. Kang, J.-G.; Sohn, Y. Interfacial nature of Ag nanoparticles supported on TiO$_2$ photocatalysts. *J. Mater. Sci.* **2011**, *47*, 824–832. [CrossRef]

230. Zhang, L.; Mohamed, H.H.; Dillert, R.; Bahnemann, D. Kinetics and mechanisms of charge transfer processes in photocatalytic systems: A review. *J. Photochem. Photobiol. C* **2012**, *13*, 263–276. [CrossRef]

231. Mohamed, H.H.; Bahnemann, D.W. The role of electron transfer in photocatalysis: Fact and fictions. *Appl. Catal. B* **2012**, *128*, 91–104. [CrossRef]

232. Wang, Z.; Li, C.; Domen, K. Recent developments in heterogeneous photocatalysts for solar-driven overall water splitting. *Chem. Soc. Rev.* **2019**, *48*, 2109–2125. [CrossRef] [PubMed]

233. Wei, Z.; Janczarek, M.; Endo, M.; Wang, K.; Balcytis, A.; Nitta, A.; Mendez-Medrano, M.G.; Colbeau-Justin, C.; Juodkazis, S.; Ohtani, B.; et al. Noble metal-modified faceted anatase titania photocatalysts: Octahedron versus decahedron. *Appl. Catal. B* **2018**, *237*, 574–587. [CrossRef] [PubMed]

234. Sreethawong, T.; Yoshikawa, S. Impact of Pt loading methods over mesoporous-assembled TiO$_2$–ZrO$_2$ mixed oxide nanocrystal on photocatalytic dye-sensitized H$_2$ production activity. *Mater. Res. Bull.* **2012**, *47*, 1385–1395. [CrossRef]

235. Kraeutler, B.; Bard, A.J. Heterogeneous photocatalytic preparation of supported catalysts. Photodeposition of platinum on titanium dioxide powder and other substrates. *J. Am. Chem. Soc.* **1978**, *100*, 4317–4318. [CrossRef]

236. Kumar, S.G.; Rao, K.S.R.K. Comparison of modification strategies towards enhanced charge carrier separation and photocatalytic degradation activity of metal oxide semiconductors (TiO$_2$, WO$_3$ and ZnO). *Appl. Surf. Sci.* **2017**, *391*, 124–148. [CrossRef]

237. Chen, H.W.; Ku, Y.; Kuo, Y.L. Effect of Pt/TiO$_2$ characteristics on temporal behavior of o-cresol decomposition by visible light-induced photocatalysis. *Water Res.* **2007**, *41*, 2069–2078. [CrossRef] [PubMed]

238. Li, J.; Xu, J.; Dai, W.-L.; Fan, K. Dependence of Ag deposition methods on the photocatalytic activity and surface state of TiO$_2$ with twistlike helix structure. *J. Phys. Chem. C* **2009**, *113*, 8343–8349. [CrossRef]

239. Elghniji, K.; Hentati, O.; Mlaik, N.; Mahfoudh, A.; Ksibi, M. Photocatalytic degradation of 4-chlorophenol under P-modified TiO$_2$/UV system: Kinetics, intermediates, phytotoxicity and acute toxicity. *J. Environ. Sci.* **2012**, *24*, 479–487. [CrossRef]

240. Yoshida, H. Photocatalytic organic syntheses. In *Environmentally Benign Photocatalysts*; Anpo, M., Kamat, P.V., Eds.; Springer: New York, NY, USA, 2010; pp. 647–669. [CrossRef]

241. Szczepanik, B. Photocatalytic degradation of organic contaminants over clay-TiO$_2$ nanocomposites: A review. *Appl. Clay Sci.* **2017**, *141*, 227–239. [CrossRef]

242. Vasseghian, Y.; Khataee, A.; Dragoi, E.-N.; Moradi, M.; Nabavifard, S.; Oliveri Conti, G.; Mousavi Khaneghah, A. Pollutants degradation and power generation by photocatalytic fuel cells: A comprehensive review. *Arab. J. Chem.* **2020**, *13*, 8458–8480. [CrossRef]

243. Benz, D.; Felter, K.M.; Koser, J.; Thoming, J.; Mul, G.; Grozema, F.C.; Hintzen, H.T.; Kreutzer, M.T.; van Ommen, J.R. Assessing the role of Pt clusters on TiO$_2$ (P25) on the photocatalytic degradation of Acid Blue 9 and Rhodamine B. *J. Phys. Chem. C* **2020**, *124*, 8269–8278. [CrossRef]

244. Ajmal, A.; Majeed, I.; Malik, R.N.; Idriss, H.; Nadeem, M.A. Principles and mechanisms of photocatalytic dye degradation on TiO$_2$ based photocatalysts: A comparative overview. *RSC Adv.* **2014**, *4*, 37003–37026. [CrossRef]

245. Qourzal, S.; Barka, N.; Tamimi, M.; Assabbane, A.; Nounah, A.; Ihlal, A.; Ait-Ichou, Y. Sol–gel synthesis of TiO$_2$–SiO$_2$ photocatalyst for β-naphthol photodegradation. *Mater. Sci. Eng. C* **2009**, *29*, 1616–1620. [CrossRef]

246. Antharjanam, S.; Philip, R.; Suresh, D. Photocatalytic degradation of wastewater pollutants: Titanium dioxide mediated degradation of methyl orange and beta-naphthol orange. *Ann. Chim.* **2003**, *93*, 719–728.

247. Hashimoto, K.; Kawai, T.; Sakata, T. Photocatalytic reactions of hydrocarbons and fossil-fuels with water—Hydrogen production and oxidation. *J. Phys. Chem.* **1984**, *88*, 4083–4088. [CrossRef]

248. Kim, J.; Choi, W. Hydrogen producing water treatment through solar photocatalysis. *Energy Environ. Sci.* **2010**, *3*, 1042. [CrossRef]

249. Yuzawa, H.; Kumagai, J.; Yoshida, H. Reaction mechanism of aromatic ring amination of benzene and substituted benzenes by aqueous ammonia over platinum-loaded titanium oxide photocatalyst. *J. Phys. Chem. C* **2013**, *117*, 11047–11058. [CrossRef]

250. Yuzawa, H.; Aoki, M.; Otake, K.; Hattori, T.; Itoh, H.; Yoshida, H. Reaction mechanism of aromatic ring hydroxylation by water over platinum-loaded titanium oxide photocatalyst. *J. Phys. Chem. C* **2012**, *116*, 25376–25387. [CrossRef]

251. Yoshida, H.; Yuzawa, H.; Aoki, M.; Otake, K.; Itoh, H.; Hattori, T. Photocatalytic hydroxylation of aromatic ring by using water as an oxidant. *Chem. Commun.* **2008**, 4634–4636. [CrossRef] [PubMed]

252. Mancuso, A.; Sacco, O.; Sannino, D.; Venditto, V.; Vaiano, V. One-step catalytic or photocatalytic oxidation of benzene to phenol: Possible alternative routes for phenol synthesis? *Catalysts* **2020**, *10*, 1424. [CrossRef]

253. Kim, J.; Lee, J.; Choi, W. Synergic effect of simultaneous fluorination and platinization of TiO$_2$ surface on anoxic photocatalytic degradation of organic compounds. *Chem. Commun.* **2008**, 756–758. [CrossRef]

254. Sola, A.C.; Homs, N.; Ramírez de la Piscina, P. Photocatalytic H$_2$ production from ethanol$_{(aq)}$ solutions: The effect of intermediate products. *Int. J. Hydrog. Energy* **2016**, *41*, 19629–19636. [CrossRef]

255. Cho, Y.-J.; Kim, H.-i.; Lee, S.; Choi, W. Dual-functional photocatalysis using a ternary hybrid of TiO$_2$ modified with graphene oxide along with Pt and fluoride for H$_2$-producing water treatment. *J. Catal.* **2015**, *330*, 387–395. [CrossRef]

256. Zhang, X.; Deng, J.; Yan, J.; Song, Y.; Mo, Z.; Qian, J.; Wu, X.; Yuan, S.; Li, H.; Xu, H. Cryo-mediated liquid-phase exfoliated 2D BP coupled with 2D C$_3$N$_4$ to photodegradate organic pollutants and simultaneously generate hydrogen. *Appl. Surf. Sci.* **2019**, *490*, 117–123. [CrossRef]

257. Jiang, X.-H.; Wang, L.-C.; Yu, F.; Nie, Y.-C.; Xing, Q.-J.; Liu, X.; Pei, Y.; Zou, J.-P.; Dai, W.-L. Photodegradation of organic pollutants coupled with simultaneous photocatalytic evolution of hydrogen using quantum-dot-modified g-C$_3$N$_4$ catalysts under visible-light irradiation. *ACS Sustain. Chem. Eng.* **2018**, *6*, 12695–12705. [CrossRef]

258. Mogyorósi, K.; Kmetykó, Á.; Czirbus, N.; Veréb, G.; Sipos, P.; Dombi, A. Comparison of the substrate dependent performance of Pt−-, Au- and Ag-doped TiO$_2$ photocatalysts in H$_2$-production and in decomposition of various organics. *React. Kinet. Catal. Lett.* **2009**, *98*, 215–225. [CrossRef]

259. Vaiano, V.; Iervolino, G. Photocatalytic removal of methyl orange azo dye with simultaneous hydrogen production using Ru-modified ZnO photocatalyst. *Catalysts* **2019**, *9*, 964. [CrossRef]

260. Chu, K.H.; Ye, L.; Wang, W.; Wu, D.; Chan, D.K.L.; Zeng, C.; Yip, H.Y.; Yu, J.C.; Wong, P.K. Enhanced photocatalytic hydrogen production from aqueous sulfide/sulfite solution by ZnO$_{0.6}$S$_{0.4}$ with simultaneous dye degradation under visible-light irradiation. *Chemosphere* **2017**, *183*, 219–228. [CrossRef] [PubMed]

261. Patsoura, A.; Kondarides, D.I.; Verykios, X.E. Enhancement of photoinduced hydrogen production from irradiated Pt/TiO$_2$ suspensions with simultaneous degradation of azo-dyes. *Appl. Catal. B* **2006**, *64*, 171–179. [CrossRef]

262. Wu, C.; Yin, M.; Zhang, R.; Li, Z.; Zou, Z.; Li, Z. Further studies of photodegradation and photocatalytic hydrogen production over Nafion-coated Pt/P25 sensitized by rhodamine B. *Int. J. Hydrog. Energy* **2020**, *45*, 22700–22710. [CrossRef]

263. Mills, A.; Lee, S.K. Platinum group metals and their oxides in semiconductor photosensitisation. *Platinum Met. Rev.* **2003**, *47*, 2–12.

264. Montoya, J.F.; Velásquez, J.A.; Salvador, P. The direct–indirect kinetic model in photocatalysis: A reanalysis of phenol and formic acid degradation rate dependence on photon flow and concentration in TiO$_2$ aqueous dispersions. *Appl. Catal. B* **2009**, *88*, 50–58. [CrossRef]

265. Monllor-Satoca, D.; Gómez, R.; González-Hidalgo, M.; Salvador, P. The "Direct–Indirect" model: An alternative kinetic approach in heterogeneous photocatalysis based on the degree of interaction of dissolved pollutant species with the semiconductor surface. *Catal. Today* **2007**, *129*, 247–255. [CrossRef]

266. Kim, J.; Park, Y.; Park, H. Solar hydrogen production coupled with the degradation of a dye pollutant using TiO$_2$ modified with platinum and nafion. *Int. J. Photoenergy* **2014**, *2014*, 1–9. [CrossRef]

267. Howsam, M.; Jones, K.C. Sources of PAHs in the environment. In *PAHs and Related Compounds*; Neilson, A.H., Ed.; Springer: Berlin/Heidelberg, Germany, 1998; pp. 137–174. [CrossRef]

268. Soana, F.; Sturini, M.; Cermenati, L.; Albini, A. Titanium dioxide photocatalyzed oxygenation of naphthalene and some of its derivatives. *J. Chem. Soc. Perkin Trans.* **2000**, 699–704. [CrossRef]

269. Rubio-Clemente, A.; Torres-Palma, R.A.; Penuela, G.A. Removal of polycyclic aromatic hydrocarbons in aqueous environment by chemical treatments: A review. *Sci. Total Environ.* **2014**, *478*, 201–225. [CrossRef] [PubMed]

270. Hykrdová, L.; Jirkovský, J.; Mailhot, G.; Bolte, M. Fe(III) photoinduced and Q-TiO$_2$ photocatalysed degradation of naphthalene: Comparison of kinetics and proposal of mechanism. *J. Photochem. Photobiol. A* **2002**, *151*, 181–193. [CrossRef]

271. Lair, A.; Ferronato, C.; Chovelon, J.-M.; Herrmann, J.-M. Naphthalene degradation in water by heterogeneous photocatalysis: An investigation of the influence of inorganic anions. *J. Photochem. Photobiol. A* **2008**, *193*, 193–203. [CrossRef]

272. Al-Madanat, O.; Curti, M.; Günnemann, C.; Alsalka, Y.; Dillert, R.; Bahnemann, D.W. TiO$_2$ photocatalysis: Impact of the platinum loading method on reductive and oxidative half-reactions. *Catal. Today*. (Under Review).